

Microscopic origin of spin-orbital separation in Sr_2CuO_3

Krzysztof Wohlfeld,^{1,2} Satoshi Nishimoto,² Maurits W. Haverkort,^{3,4,5} and Jeroen van den Brink^{2,6}

¹*Stanford Institute for Materials and Energy Sciences,
SLAC National Laboratory and Stanford University,
2575 Sand Hill Road, Menlo Park, CA 94025, USA*

²*Institute for Theoretical Solid State Physics, IFW Dresden, D-01069 Dresden, Germany*

³*Max-Planck-Institut für Festkörperforschung, D-70569 Stuttgart, Germany*

⁴*Department of Physics and Astronomy, University of British Columbia, Vancouver, Canada V6T-1Z1*

⁵*Max Planck Institute for Chemical Physics of Solids, D-01187 Dresden, Germany*

⁶*Department of Physics, TU Dresden, D-01062 Dresden, Germany*

(Dated: August 8, 2021)

Recently performed resonant inelastic x-ray scattering experiment (RIXS) at the copper L_3 edge in the quasi-1D Mott insulator Sr_2CuO_3 has revealed a significant dispersion of a single orbital excitation (orbiton). This large and unexpected orbiton dispersion has been explained using the concept of spin-orbital fractionalization in which the orbiton, which is intrinsically coupled to the spinon in this material, liberates itself from the spinon due to the strictly 1D nature of its motion. Here we investigate this mechanism in detail by: (i) deriving the microscopic spin-orbital superexchange model from the charge transfer model for the CuO_3 chains in Sr_2CuO_3 , (ii) mapping the orbiton motion in the obtained spin-orbital model into a problem of a single hole moving in an effective half-filled antiferromagnetic chain t - J model, and (iii) solving the latter model using the exact diagonalization and obtaining the orbiton spectral function. Finally, the RIXS cross section is calculated based on the obtained orbiton spectral function and compared with the RIXS experiment.

PACS numbers: 75.25.Dk, 75.30.Ds, 71.10.Fd, 78.70.Ck

I. INTRODUCTION

Long and difficult ‘search’ for orbitons.— A relatively well-understood problem in strongly correlated electrons systems concerns the propagation of collective magnetic (spin) excitations in Mott insulators such as e.g. 3D LaMnO_3 , 2D La_2CuO_4 , ladder SrCu_2O_3 , and 1D Sr_2CuO_3 ¹. The theoretically calculated dispersion of such magnetic excitations (magnons in 2D or 3D, triplons in the ladder, or spinons in 1D) agrees very well with the one measured using the inelastic neutron scattering^{2–4} or the resonant inelastic x-ray scattering (RIXS)^{5–8}. The origin of this fact is the relative simplicity of the spin-spin interactions, which are usually modeled using the Heisenberg-type spin Hamiltonians^{1,2}. The excitation spectrum of such Hamiltonians can then be obtained using e.g. the linear spin wave approximation in 2D/3D⁹ or the Bethe-Ansatz-based approaches in 1D^{9,10}.

This situation is very different when one considers propagation of the collective orbital interactions – the orbitons¹¹ (coined as such in Ref. 12). On the experimental side, this originates from the lack of experimental probe to measure orbiton dispersion^{13–15}. Even if neutrons *do* couple to the orbital excitations¹⁶ and can in principle detect orbital waves¹⁷, this cannot be easily realized experimentally¹⁸. This is due to the *usually* low transfers of energy in the neutron scattering experiments w.r.t. the energies needed to trigger the orbital excitations (for an exception see Ref. 19). Inelastic light scattering in the form of (optical) Raman scattering cannot transfer much momentum to orbital excitations leading to controversial interpretations of the observed features^{17,20,21}. Only re-

cently it has been proposed^{13,14} and then experimentally and theoretically established²² that RIXS may be used to probe the orbitons’ motion. Therefore, till last year, there were just three experimental indications of the existence of mobile orbitons: (i) indirectly in the form of Davydov splittings²³ in Cr_2O_3 , (ii) more recently and also indirectly in a pump-probe experiment in the doped manganite²⁴, and (iii) in the RIXS spectrum on titanates, where a very small (w.r.t. the experimental resolution) dispersion was found²⁵.

From the theoretical side the situation is also complex. To understand the orbiton dispersion one has to take into account the interaction between orbitons and (i) the lattice (phonons) and (ii) the spin degrees of freedom. Although the former has been investigated in several studies^{26–28} and for long ‘blamed’ for causing a confinement of the orbiton motion^{26–28}, it turned out not to be of great importance in the here discussed case of orbitons in Sr_2CuO_3 ²². Therefore, while still far from being understood, the interaction with the lattice will not be discussed in what follows. At the same time, however, the spin-orbital interaction²⁹, which stems from the inherent entanglement of the spin and orbital degrees of freedom^{30–33} in the Kugel-Khomskii superexchange (and/or direct exchange)^{11,34} models, which describe the propagation of spin or orbital excitations¹¹, has a profound impact on the orbiton motion^{13,17,35–39}. Moreover, as already discussed in Refs. 40–48, and in direct relevance to the here discussed problem in Refs. 22,49 (see also below), in order to correctly describe the collective orbital excitations, this interaction should not be treated on a mean-field level. This latter feature of the spin-orbital interaction severely complicates matter and is one of the

main motivations for the study presented in this paper.

Recent experimental and theoretical findings.— This brief overview of the problems with finding mobile orbitons, makes it clear that the recent experimental finding of the mobile orbiton in Sr_2CuO_3 ²² and its short theoretical description in Refs. 22,49, signifies a breakthrough in the study of orbital excitations. We therefore briefly summarize these findings below.

The RIXS measurements performed at copper L_3 edge in Sr_2CuO_3 ²² revealed two dispersive orbital excitations (due to large crystal field splitting also called dd excitations). Firstly, the d_{xz} orbital excitation, which (in the here used hole language) corresponds to a transfer of a hole from the ground state $d_{x^2-y^2}$ orbital to the excited d_{xz} excitation, showed a sine-like dispersion. This dispersion was of the order of 200 meV, had a dominant π period component, and a large incoherent spectrum which lead to peculiar ‘oval’-like features in the RIXS spectrum, see Fig. 1 in Ref. 22. Secondly, also the d_{xy} orbital excitation had a small dispersion with visible π period component. Finally, the other two orbital excitations (the d_{yz} and the $d_{3z^2-r^2}$ orbital excitations) did not show any significant dispersion.

While these experimental results are the first unambiguous observation of an orbiton (cf. discussion above), they turned out to constitute a challenge from a theoretical perspective. It was shown²² that the above mentioned particular features of dispersion could only be explained if the concept of spin-orbital separation was invoked and applied⁴⁹. In short, this concept suggests that: (i) the orbiton in Sr_2CuO_3 is so strongly coupled to the spin excitations (spinons in this 1D case) that its coherent motion can only be explained if this coupling was explicitly taken into account, (ii) during its motion the orbiton can nevertheless ‘liberate’ from the spinon. This scenario can explain the reason why this orbiton dispersion was not observed before: Since (on one hand) the spin-orbital separation phenomenon is rather unique to 1D and (on the other hand) the experimental searches were constrained to mostly 2D or 3D compounds, the orbiton was finally only observed when the attention was turned into a purely 1D system.

Aim and plan of the paper.— In this paper we show how to apply the spin-orbital separation concept developed and discussed in Refs. 22,49 to the problem of the orbiton motion in Sr_2CuO_3 . We start from (Sec. II) the proper charge transfer model for Sr_2CuO_3 supplemented by the terms which describe the dynamics of the excited orbitals. From this model we derive in Sec. III the corresponding ‘Kugel-Khomskii’ spin-orbital model which describes the spin and orbital dynamics in Sr_2CuO_3 , and thus defines the Hamiltonian that is used to calculate the orbiton spectral function. In Sec. IV, we calculate the orbiton spectral function using the newly developed concept of spin-orbital separation⁴⁹. Next, in Sec. V we establish the relation between the RIXS cross section and the orbiton spectral function calculated in Sec. IV and compare the obtained RIXS spectra with those obtained

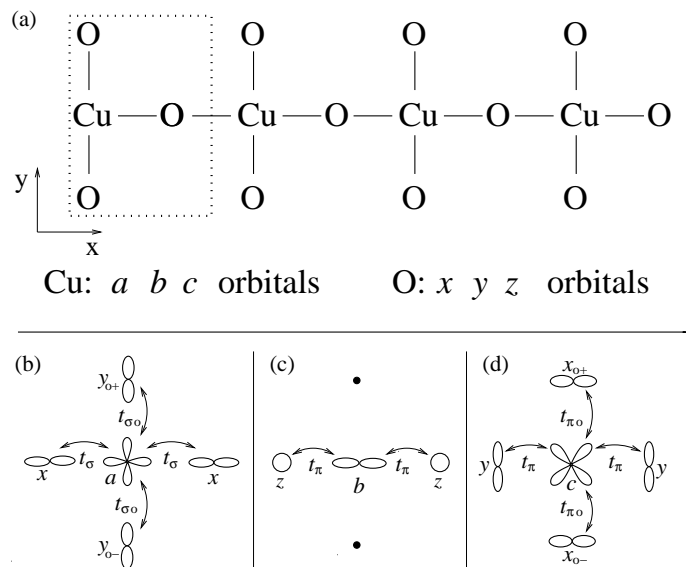


FIG. 1: The relevant atoms and orbitals that are taken into account in model Eq. (1): (a) orientation of the CuO_3 chain with one Cu site and three O sites in the unit cell (dotted line), (b) nearest neighbor O orbitals which hybridize with the Cu a orbital following Eq. (2), (c) nearest neighbor O orbitals which hybridize with the Cu b orbital following Eq. (2) – note that there is no hybridization between O orbitals that lie above / below the Cu-O-Cu-O... chain, and (d) nearest neighbor O orbitals which hybridize with the Cu c orbital following Eq. (2).

in the experiment²². Finally, in Sec. VI we discuss the possible other scenarios which might explain the experimental results presented in Ref. 22 and end with the concluding remarks.

The paper is supplemented by three appendices in which: (i) we discuss some details of the calculations performed in Sec. III A (App. A), (ii) we compare the results of Sec. IV and Sec. V to those obtained using the linear orbital wave theory (App. B), and (iii) we compare the results of Sec. V with those obtained assuming all orbital excitations to be dispersionless (App. C).

II. THE CHARGE TRANSFER MODEL

A. Hamiltonian

As noted in Sec. I the purpose of the present study is to describe the propagation of orbital excitation in the quasi-1D cuprate Sr_2CuO_3 ^{50–52}. Therefore, as our starting point we take the following multiband charge transfer Hamiltonian (which is an extended version of the charge transfer model discussed in Ref. 53):

$$\mathcal{H} = \mathcal{H}_0 + \mathcal{H}_1 + \mathcal{H}_2 + \mathcal{H}_3, \quad (1)$$

with \mathcal{H}_0 the tight binding Hamiltonian written in a basis consisting of five $3d$ orbitals per Cu site and three $2p$

orbitals per O site. The many body interactions are included in \mathcal{H}_1 , \mathcal{H}_2 , and \mathcal{H}_3 (on-site Coulomb interaction on Cu atoms, on-site Coulomb interaction on O atoms, and nearest neighbor Coulomb interaction between electrons on Cu and O site). In second quantized form and using the hopping parameters as indicated in Fig. 1 we obtain:

– for the tight binding Hamiltonian \mathcal{H}_0

$$\begin{aligned}
\mathcal{H}_0 = & -t_\sigma \sum_{i,\sigma} \left(f_{ia\sigma}^\dagger f_{ix\sigma} - f_{i+1,a\sigma}^\dagger f_{ix\sigma} + \text{H.c.} \right) \\
& -t_{\sigma o} \sum_{i,\sigma} \left(f_{ia\sigma}^\dagger f_{iy o+\sigma} - f_{ia\sigma}^\dagger f_{iy o-\sigma} + \text{H.c.} \right) \\
& -t_\pi \sum_{i,\sigma} \left(f_{ic\sigma}^\dagger f_{iy\sigma} - f_{i+1,c\sigma}^\dagger f_{iy\sigma} + f_{ib\sigma}^\dagger f_{iz\sigma} \right. \\
& \quad \left. - f_{i+1,b\sigma}^\dagger f_{iz\sigma} + \text{H.c.} \right) \\
& -t_{\pi o} \sum_{i,\sigma} \left(f_{ic\sigma}^\dagger f_{ix o+\sigma} - f_{ic\sigma}^\dagger f_{ix o-\sigma} + \text{H.c.} \right) \\
& +\Delta_x \sum_i (n_{ix} - n_{ia}) + \Delta_y \sum_i (n_{iy} - n_{ic}) \\
& +\Delta_z \sum_i (n_{iz} - n_{ib}) + \Delta_{yo} \sum_i (n_{iy o+} - n_{ia}) \\
& +\Delta_{xo} \sum_i (n_{iy o-} - n_{ia}) + \Delta_{xo} \sum_i (n_{ix o+} - n_{ib}) \\
& +\Delta_{xo} \sum_i (n_{ix o-} - n_{ib}) \\
& +\varepsilon_a \sum_i n_{ia} + \varepsilon_b \sum_i n_{ib} + \varepsilon_c \sum_i n_{ic}, \quad (2)
\end{aligned}$$

– for the on-site Coulomb repulsion on copper sites term

$$\begin{aligned}
\mathcal{H}_1 = & \sum_{i,\sigma,\alpha<\beta} (U - J_H^{\alpha\beta}) n_{i\alpha\sigma} n_{i\beta\bar{\sigma}} + \sum_{i,\sigma,\alpha<\beta} (U - 2J_H^{\alpha\beta}) n_{i\alpha\sigma} n_{i\beta\sigma} \\
& + U \sum_{i,\alpha} n_{i\alpha\uparrow} n_{i\alpha\downarrow} - \sum_{i,\sigma,\alpha<\beta} J_H^{\alpha\beta} f_{i\alpha\sigma}^\dagger f_{i\alpha\bar{\sigma}} f_{i\beta\bar{\sigma}}^\dagger f_{i\beta\sigma} \\
& + \sum_{i,\alpha<\beta} J_H^{\alpha\beta} f_{i\alpha\uparrow}^\dagger f_{i\alpha\downarrow}^\dagger f_{i\beta\downarrow} f_{i\beta\uparrow}, \quad (3)
\end{aligned}$$

– for the on-site Coulomb repulsion on oxygen sites the Hamiltonian

$$\begin{aligned}
\mathcal{H}_2 = & \sum_{i,\sigma,\mu<\nu} (U_p - J_H^{\mu\nu}) n_{i\mu\sigma} n_{i\nu\bar{\sigma}} + \sum_{i,\sigma,\mu<\nu} (U_p - 2J_H^{\mu\nu}) n_{i\mu\sigma} n_{i\nu\sigma} \\
& + U_p \sum_{i,\mu} n_{i\mu\uparrow} n_{i\mu\downarrow} - \sum_{i,\sigma,\mu<\nu} J_H^{\mu\nu} f_{i\mu\sigma}^\dagger f_{i\mu\bar{\sigma}} f_{i\nu\bar{\sigma}}^\dagger f_{i\nu\sigma} \\
& + \sum_{i,\mu<\nu} J_H^{\mu\nu} f_{i\mu\uparrow}^\dagger f_{i\mu\downarrow}^\dagger f_{i\nu\downarrow} f_{i\nu\uparrow}, \quad (4)
\end{aligned}$$

– for the nearest neighbor Coulomb repulsion

$$\mathcal{H}_3 = V_{dp} \sum_{i,\mu\alpha} n_{i\alpha} (n_{i\mu} + n_{i\mu+} + n_{i\mu-} + n_{i+1\mu}). \quad (5)$$

Here one needs to consider that

- the CuO_3 chain is oriented along the x axis (Cu-Cu distance is set to 1), cf. Fig. 1(a); for simplicity hole notation is used;
- the charge transfer model unit cell [cf. Fig. 1(a)] includes: (i) one copper atom with three $3d$ orbitals: $3d_{x^2-y^2} \equiv a$, $3d_{zx} \equiv b$, and $3d_{xy} \equiv c$, (ii) one oxygen atom within the Cu-O-Cu-O-... chain with three $2p$ orbitals: $2p_x \equiv x$, $2p_y \equiv y$, $2p_z \equiv z$, (iii) two equivalent oxygen atoms outside the Cu-O-Cu-O-... chain with two $2p$ orbitals: above this chain $-2p_x \equiv xo+$, $2p_y \equiv yo+$ and below this chain $-2p_x \equiv xo-$, $2p_y \equiv yo-$;
- the copper orbital indices are $\alpha, \beta \in \{a, b, c\}$, the chain oxygen orbital indices are $\mu, \nu \in \{x, y, z\}$, and the spin index $\sigma \in \{\uparrow, \downarrow\}$ ($\bar{\sigma} = -\sigma$);
- $f_{i\kappa\sigma}$ annihilates a hole at site i in orbital κ with spin σ while density operators are $n_{i\kappa} = n_{i\kappa\uparrow} + n_{i\kappa\downarrow}$ with $n_{i\kappa\sigma} = f_{i\kappa\sigma}^\dagger f_{i\kappa\sigma}$;
- the structure of the dominant hopping elements follows the Slater-Koster scheme (and was verified by our LDA calculations) and is depicted in Fig. 1(b)-(d); the rather large hopping between oxygens $t_{pp'}$ (cf. Ref. 53) is neglected; although this may give rise to a significantly smaller hole occupation on copper sites (and consequently may reduce the *intensity* of the dispersive dd excitations), in the approach presented below it will not contribute to the superexchange processes;
- the charge transfer energy Δ_μ is measured for the particular $2p$ orbital from the relevant $3d$ orbital (in the here used hole notation, see also above), i.e. from that $3d$ orbital which hybridizes with this particular $2p$ orbital;
- due to crystal field there are distinct on-site energies ε_α for each $3d$ orbital;
- the structure of the Coulomb interaction follows Refs. 54,55 and up to two-orbital interaction terms exactly reproduces the correct on-site Coulomb interaction; note that the Coulomb interaction on oxygens above and below the chain is not considered because we are interested merely in the Mott insulating case with one hole per copper site and in the analysis that follows *this particular* Coulomb interaction plays only a minor role.

We note at this point that the above model does not contain the $d_{yz} \equiv d$ and $d_{3z^2-r^2} \equiv e$ orbitals. This is because there will not be any sizable dispersion due to the very small superexchange processes for the dd excitations involving these orbitals. Note further that: (i) the hopping from the d_{yz} orbital to the neighboring oxygen along the chain direction x is negligible, and (ii) the hopping from the $d_{3z^2-r^2}$ to the p_x orbital on the neighboring oxygen is particularly small in this compound (much

smaller than t_π according to our LDA calculations). We will therefore include these orbitals only when calculating the RIXS cross section in Sec. V.

B. Parameters

In the model Hamiltonian Eq. (1) a large number of parameters appear, which need to be fixed in order to obtain quantitative results that can be compared to experiment, cf. left column of Table I.

In principle we used the basic set of the parameters that was proposed in Ref. 53. The only exception is the intersite Coulomb repulsion V_{dp} which is set to a somewhat smaller value of 1 eV than the exceptionally large one suggested in Ref. 53. Note however, that the smaller value is still generally accepted for the cuprates⁵⁶. Besides, this value leads to the spin superexchange parameter that is equal to 0.24 eV (see below), which is the experimentally observed value²². Finally, we used the following values for parameters not considered in Ref. 53:

(i) The Hund's exchange J_H^c and J_H^b are calculated using Slater integrals from Ref. 57 while J_H^p is taken from Ref. 56.

(ii) ε_b and ε_c are estimated to be 0.5 eV from the LDA calculations.

(iii) While following Ref. 53 $\Delta_x = 3.0$ eV and $\Delta_{y0} = 3.5$ eV, the values of the other charge transfer parameters are not given in this reference and have to be obtained in another way. It seems reasonable to assume first that values of Δ_{xo} , Δ_y , and Δ_z are roughly of the order of Δ_x . But, since the charge transfer parameters are defined as equal to the difference in energy between the particular hybridizing c or b orbital and the particular $2p$ orbital, they have to be lower than Δ_x . Quantum chemical calculations suggest, however, that the actual values of Δ_y and Δ_z might still be different: it occurs that the values of the on-site energies of the b and c orbital are not identical and that the b orbital has a higher energy than the c orbital by ca. 0.7 eV, cf. Ref. 22. Altogether, this suggests the following values for these two parameters: $\Delta_y = 2.8$ eV and $\Delta_z = 2.2$ eV. We will show later that these values give the orbital dispersion in reasonably good agreement with the RIXS experiment²².

(iv) t_π and $t_{\pi o}$ are assumed to be roughly of the order of 55% of t_σ and $t_{\sigma o}$ (respectively)⁵⁶.

Note that Table I contains also a few other parameters which are later introduced in this paper. While they mostly follow from the charge transfer model parameters mentioned above, we will comment on their origin once they become relevant in the following sections.

III. DERIVATION OF THE SPIN-ORBITAL MODEL

Since the Coulomb repulsion U and the charge transfer energies Δ_μ present in model Eq. (1) are far larger

than the hoppings t_n ($t_n \ll U$ and $t_n \ll \Delta_\mu$ where $n = \sigma, \pi, \sigma o, \pi o$), cf. Table I, the ground state of \mathcal{H} is a Mott insulator. This is because, in the zeroth order approximation in the perturbation theory in hopping t_n and in the regime of one hole per copper site, there is one hole localized in the a orbital at each copper site i . Similarly, when a single orbital excitations is made, then in the zeroth order the hole will be localized on a single copper site in a particular b or c orbital (because the charge transfer energy Δ_μ is always positive).

In the second and fourth order perturbation theory in t_n (the terms obtained from t_n and t_n^3 perturbation vanish⁵⁸) the hole can delocalize which leads to a particular low energy Hamiltonian – the spin-orbital Hamiltonian. This Hamiltonian has the following generic structure:

$$\bar{\mathcal{H}} = \bar{\mathcal{H}}_0 + \bar{\mathcal{H}}_a + \bar{\mathcal{H}}_b + \bar{\mathcal{H}}_c. \quad (6)$$

It consists of two kinds of terms: (i) $\bar{\mathcal{H}}_0$ which is a result of the second order perturbation theory in t_n , and (ii) $\bar{\mathcal{H}}_a + \bar{\mathcal{H}}_b + \bar{\mathcal{H}}_c$ terms which follow from the fourth order perturbation theory in t_n and can be called ‘superexchange’ terms. Note that the latter terms can be classified in two classes: (i) $\bar{\mathcal{H}}_a$ – the so-called ‘standard’ or ‘spin’ superexchange terms, which contribute when all holes are in the a orbitals (i.e. no orbital excitations are present), and (ii) $\bar{\mathcal{H}}_b + \bar{\mathcal{H}}_c$ – the spin-orbital superexchange (‘Kugel-Khomskii’-like) terms with one orbital excitation present on one site of the bond (in b or c orbital) and no orbital excitation present on the other site of the bond. In the following subsections we discuss these terms ‘step-by-step’.

A. Renormalization of on-site energies: $\bar{\mathcal{H}}_0$

In the second order perturbation theory in t_n the hole can delocalize to the four neighboring oxygen sites surrounding the copper sites forming bonding and antibonding states. Although there are many important consequences of such t_n^2 processes, let us now just explore one of them which actually turns out to be very important: the renormalization of the on-site energies of the orbitals. In Appendix A we discuss another, perhaps less important, consequence of these processes: the renormalization of the hopping within the chain due to hybridization with oxygen orbitals above and below the chain (these renormalization factors are called λ_a and λ_c).

When the hole delocalizes into the bonding and antibonding states formed by the a , b , or c orbitals with the four surrounding oxygen sites, the effective on-site energies of the orbital levels are strongly renormalized with respect to the energy levels of the pure a , b , or c orbitals. Although the proper calculation of this phenomenon can be done analytically by diagonalizing a five level problem defined separately for each of the copper α orbitals, we do not perform it here. Instead we take the values obtained from the Ligand Field Theory Programme⁵⁹ based on the multiplet ligand field theory using Wannier orbitals on a

TABLE I: Assumed values of the parameters used in the paper, see text for further details. All parameters except R , R_n^m and r_n^m (which are dimensionless) are given in eV. Tilde before the value of the parameter denotes the fact that this precise value is not used in the analysis.

Model parameters				Spectral function / RIXS parameters	
Charge transfer model (Sec. II)		Spin-orbital model (Sec. III)		Local excitation energies (Sec. IV, V, and App. C)	
t_σ	1.5	J_1	0.088	E_b	2.15
t_π	0.83	J_2^b	0.021	E_c	1.41
$t_{\sigma o}$	1.8	J_2^c	0.010	E_d	2.06
$t_{\pi o}$	1.0	J_{12}^b	0.043	E_e	2.44
Δ_x	3.0	J_{12}^c	0.030	E_{AF}	0.33
Δ_y	2.8	R	1.7	Effective t - J models (Sec. IV)	
Δ_z	2.2	R_1^b	2.5	t_b	0.084
Δ_{xo}	2.5	R_1^c	2.3	t_c	0.051
Δ_{yo}	3.5	R_2^b	2.0	J	0.24
U	8.8	R_2^c	1.9	Linear orbital wave approximation (App. B)	
U_p	4.4	r_1^b	1.7	B	2.48
$J_H^b \equiv J_H^{ab}$	1.2	r_1^c	1.3	C	1.74
$J_H^c \equiv J_H^{ac}$	0.69	r_2^b	1.2	J_b	-0.019
$J_H^p \equiv J_H^{\mu\nu}$	0.83	r_2^c	1.1	J_c	-0.014
V_{dp}	1.0	$\bar{\varepsilon}_a$	0.0		
ε_a	0.0	$\bar{\varepsilon}_b$	~ 2.2		
ε_b	~ 0.5	$\bar{\varepsilon}_c$	~ 2.0		
ε_c	~ 0.5				

CuO₄ cluster. It occurs that, for realistic values of parameters of model Eq. (1) (see Table I), the antibonding states are well-separated from the bonding states and we can safely neglect the latter ones in the low energy limit that is of interest here. This leads to the following term in our spin-orbital model:

$$\bar{H}_0 = \bar{\varepsilon}_a \sum_i \tilde{n}_{ia} + \bar{\varepsilon}_b \sum_i \tilde{n}_{ib} + \bar{\varepsilon}_c \sum_i \tilde{n}_{ic}, \quad (7)$$

where the values of the parameters $\bar{\varepsilon}_\alpha$ are shown in Table I. Here, we use the operators $n_{i\alpha}$ from Eq. (1), although a rigorous treatment would require the use of the operators actually creating the particular bonding states centered around a copper α orbital at site i . We discuss in Appendix A why such simplification is to a large extent justified. Besides, the tilde above the operators denotes the fact that we prohibit double occupancies in this low energy Hamiltonian due to the large on-site Hubbard U and U_p .

It is convenient to define at this point the orbital pseudospin operators: $\sigma = \frac{1}{2}$ where

$$\begin{aligned} \sigma_i^z &= \frac{1}{2}(\tilde{n}_{ib} - \tilde{n}_{ia}), \\ \sigma_i^+ &= \tilde{f}_{bi}^\dagger \tilde{f}_{ai}, \\ \sigma_i^- &= \tilde{f}_{ai}^\dagger \tilde{f}_{bi}. \end{aligned} \quad (8)$$

and $\tau = \frac{1}{2}$ where

$$\begin{aligned} \tau_i^z &= \frac{1}{2}(\tilde{n}_{ic} - \tilde{n}_{ia}), \\ \tau_i^+ &= \tilde{f}_{ci}^\dagger \tilde{f}_{ai}, \\ \tau_i^- &= \tilde{f}_{ai}^\dagger \tilde{f}_{ci}, \end{aligned} \quad (9)$$

Here the tilde above the operators denotes the fact that double occupancies are forbidden in this low energy Hamiltonian due to large on-site Coulomb repulsion U and U_p . Setting $\bar{\varepsilon}_a = 0$ we can rewrite Eq. (7) as follows

$$\bar{H}_0 = \bar{\varepsilon}_b \sum_i \left(\frac{1}{2} + \sigma_i^z \right) + \bar{\varepsilon}_c \sum_i \left(\frac{1}{2} + \tau_i^z \right). \quad (10)$$

B. Spin superexchange: \bar{H}_a

Let us firstly study the superexchange interactions when only one type of orbital is occupied along the superexchange bond. In this case it is very straightforward to show that model Eq. (1) can be easily reduced to the low energy Heisenberg model for spins $S = 1/2$ using the perturbation theory to fourth order in t_σ ⁵⁸, cf. Fig. 2:

$$\bar{H}_a = J_1(1 + R) \sum_i \mathcal{P}_{i,i+1} \left(\mathbf{S}_i \cdot \mathbf{S}_{i+1} - \frac{1}{4} \right), \quad (11)$$

where $\mathcal{P}_{i,i+1}$ denotes the fact that there are no orbital excitation present along the bond $\langle i, i+1 \rangle$ and is defined as

$$\mathcal{P}_{i,i+1} = \left(\frac{1}{2} + \tau_i^z \right) \left(\frac{1}{2} + \tau_{i+1}^z \right) \left(\frac{1}{2} + \sigma_i^z \right) \left(\frac{1}{2} + \sigma_{i+1}^z \right). \quad (12)$$

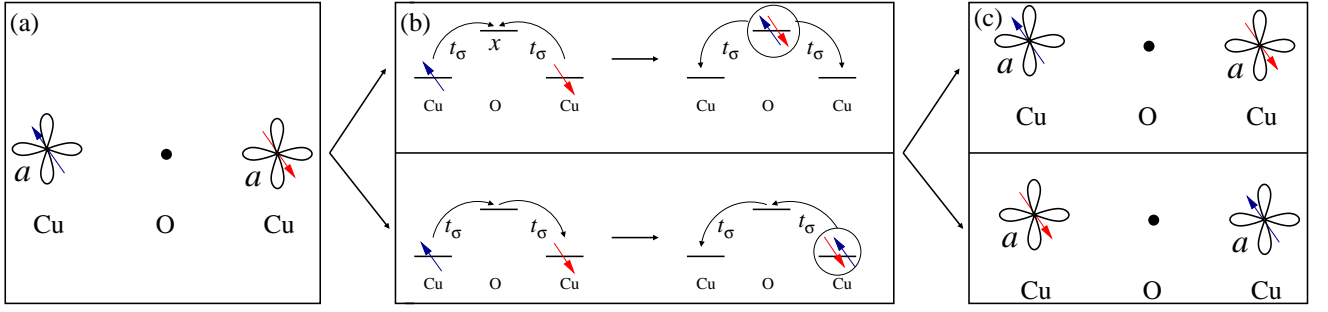


FIG. 2: (Color online) Schematic view of superexchange interactions when no orbital excitations are present, i.e. between spins (arrows) of the holes in the a orbitals: the ‘initial’ state [panel (a)] can be brought into the so-called ‘virtual’ state of the superexchange process [circle with two spins (arrows) on the right side of panel (b)] by the virtual hopping [left side of panel (b)] which can ‘decay’ [right side of panel (b)] via the virtual hopping into the ‘final’ state of the superexchange [panel (c)]. Panel (b) shows two kinds of ‘virtual’ states with doubly occupied ions: on the oxygen (copper) on the lower (upper) side of the panel with the energy cost $\propto U$ ($\propto Up + 2\Delta$), respectively. Panel (c) shows two possible low energy ‘final’ configurations without double occupancies: without spin flip (i.e. identical to the initial state) and with spin flip. Note that panel (b) shows relevant copper and oxygen orbitals in a schematic way, i.e. depicted by horizontal bars, while panels (a) and (c) explicitly show the relevant copper orbitals (oxygen orbitals are not shown on these panels).

Note that here the superexchange interactions involve not only the spin degree of freedom $S = \frac{1}{2}$:

$$\begin{aligned} S_i^z &= \frac{1}{2}(\tilde{n}_{i\uparrow} - \tilde{n}_{i\downarrow}), \\ S_i^+ &= \tilde{f}_{i\uparrow}^\dagger \tilde{f}_{i\downarrow}, \\ S_i^- &= \tilde{f}_{i\downarrow}^\dagger \tilde{f}_{i\uparrow}. \end{aligned} \quad (13)$$

but also the orbital degree of freedom pseudospin operators defined in the previous subsection. Again the tilde above the operators denotes the fact that double occupancies are forbidden in this low energy Hamiltonian due to large on-site Coulomb repulsion U and U_p .

The superexchange constant contains contributions due to charge excitations on copper sites ($\sim J_1$) and on the oxygen sites located in between the copper sites ($\sim J_1 R$), where

$$J_1 = \left(\frac{2\bar{t}_\sigma^2}{\Delta_x + V_{dp}} \right)^2 \frac{1}{U}, \quad (14)$$

with $\bar{t}_\sigma = \lambda_a t_\sigma$ (see Appendix A for origin of the factor λ_a) and

$$R = \frac{2U}{2\Delta_x + U_p}. \quad (15)$$

Two remarks are in order here. Firstly, when no orbital excitations are present, the Hamiltonian Eq. (11) is equal to the well-known spin-only Heisenberg model. This is in agreement with the ‘common wisdom’ stating that the orbital degrees of freedom can be easily integrated out in systems with only one orbital occupied in the ground state. Secondly, in the above derivation we neglected intermediate states with 1A_1 or 1E symmetry. In principle superexchange processes which involve these intermediate states should also be taken into account. However,

due to the crystal field splitting this would mean that the final states of the superexchange process would contain high energy orbital excitations. Consequently these processes are suppressed.

C. Spin-orbital superexchange for b orbital: \bar{H}_b

If along a bond there is one hole in the b orbital (due to e.g. an orbital excitation created in RIXS) and another one in the a orbital, then using the perturbation theory to fourth order in t_n we obtain (cf. Figs 3-4):

$$\begin{aligned} \bar{H}_b = & \sum_i \left(\mathbf{S}_i \cdot \mathbf{S}_{i+1} + \frac{3}{4} \right) \left[\left(R_1^b J_{12}^b + r_1^b \frac{J_1 + J_2^b}{2} \right) \right. \\ & \left. \left(\sigma_i^z \sigma_{i+1}^z - \frac{1}{4} \right) + \frac{R_1^b + r_1^b}{2} J_{12}^b (\sigma_i^+ \sigma_{i+1}^- + \sigma_i^- \sigma_{i+1}^+) \right] \\ & + \sum_i \left(\frac{1}{4} - \mathbf{S}_i \cdot \mathbf{S}_{i+1} \right) \left[\left(R_2^b J_{12}^b + r_2^b \frac{J_1 + J_2^b}{2} \right) \right. \\ & \left. \left(\sigma_i^z \sigma_{i+1}^z - \frac{1}{4} \right) - \frac{R_2^b + r_2^b}{2} J_{12}^b (\sigma_i^+ \sigma_{i+1}^- + \sigma_i^- \sigma_{i+1}^+) \right], \end{aligned} \quad (16)$$

where the superexchange constant J_1 is the one given by Eq. (14) while

$$J_2^b = \left(\frac{2t_\pi^2}{\Delta_z + V_{dp}} \right)^2 \frac{1}{U}, \quad (17)$$

and

$$J_{12}^b = \frac{(2t_\pi \bar{t}_\sigma)^2}{(\Delta_z + V_{dp})(\Delta_x + V_{dp})} \frac{1}{U}. \quad (18)$$

The complex structure of Hamiltonian (16) is a consequence of the fact that the proper derivation of such low

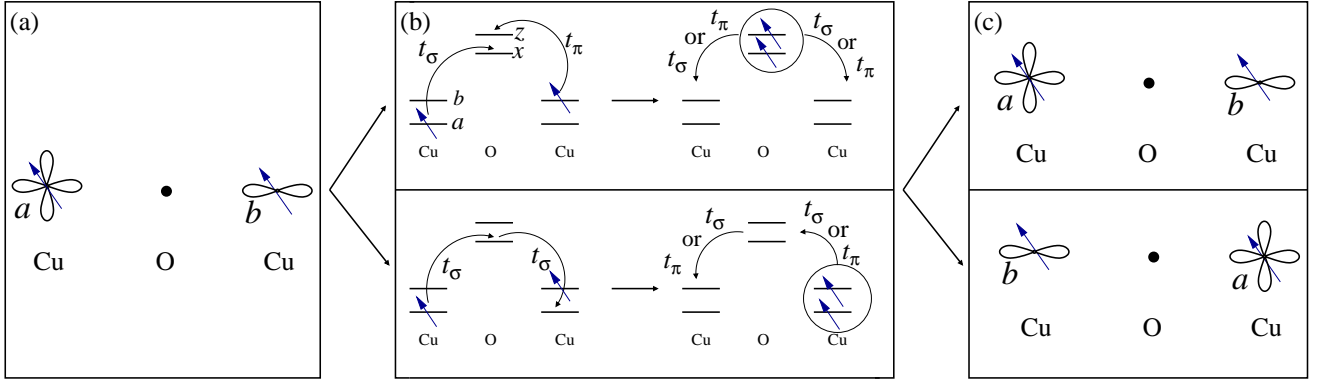


FIG. 3: (Color online) Schematic view of superexchange interactions with one orbital excitation (here: into orbital b) on one site and no orbital excitations on the other site (hole in orbital a) in the case that both spins (arrows) on the neighbouring orbitals are *parallel*: similarly as in Fig. 2 the ‘initial’ state [panel (a)] can be brought into the so-called ‘virtual’ state of the superexchange process [circle with two spins (arrows) on the right side of panel (b)] by the virtual hopping [left side of panel (b)] which can ‘decay’ [right side of panel (b)] via the virtual hopping into the ‘final’ state of the superexchange [panel (c)]. Panel (b) shows two kinds of ‘virtual’ states with doubly occupied ions – on the oxygen and copper site, cf. Fig. 2. Panel (c) shows two possible low energy ‘final’ configurations without double occupancies: without *orbital* flip (i.e. identical to the initial state) and with *orbital* flip.

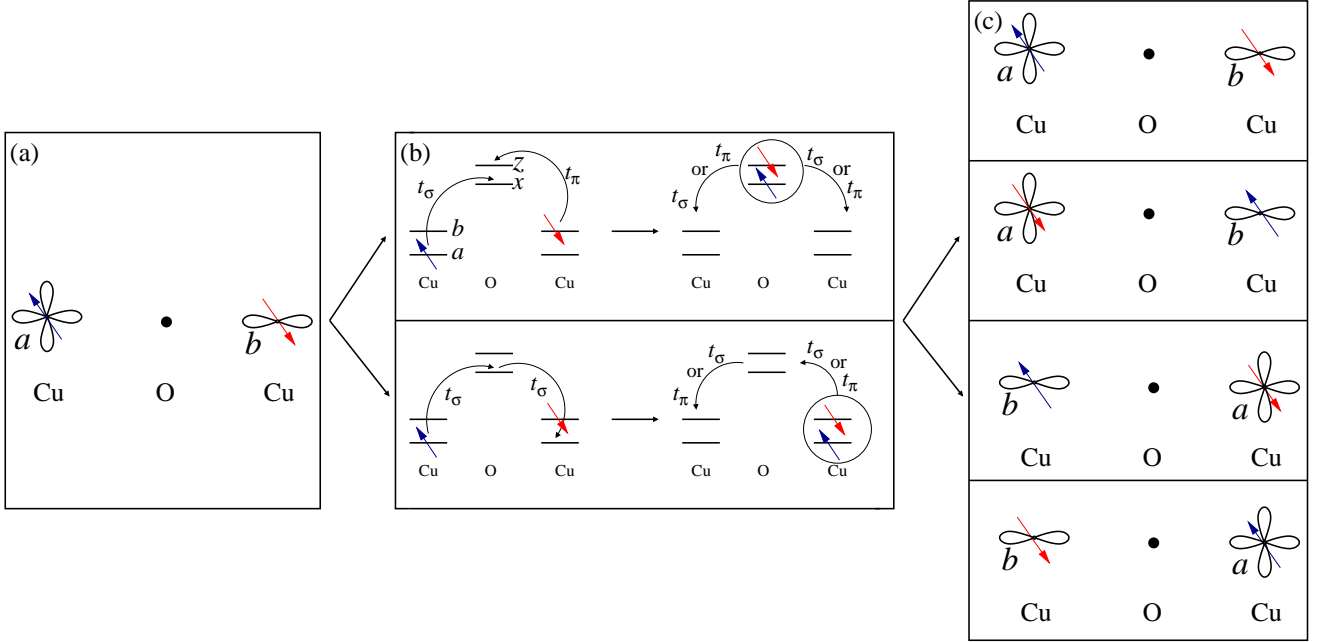


FIG. 4: (Color online) Schematic view of superexchange interactions with one orbital excitation (here: into orbital b) on one site and no orbital excitations on the other site (hole in orbital a) in the case that spins (arrows) on the neighboring orbitals are *antiparallel*: similarly as in Fig. 2 the ‘initial’ state [panel (a)] can be brought into the so-called ‘virtual’ state of the superexchange process [circle with two spins (arrows) on the right side of panel (b)] by the virtual hopping [left side of panel (b)] which can ‘decay’ [right side of panel (b)] via the virtual hopping into the ‘final’ state of the superexchange [panel (c)]. Panel (b) shows two kinds of ‘virtual’ states with doubly occupied ions – on the oxygen and copper site, cf. Fig. 2. Panel (c) shows *four* possible low energy ‘final’ configurations without double occupancies: with/without *orbital* flip and with/without *spin* flip.

energy model has to include the superexchange processes with four distinct intermediate states:

(i) The high spin state 3T_1 on copper sites (middle bottom panel of Fig. 3) which involves $d^2 = b^1a^1$ orbital configuration and with energy in terms of Racah

parameters⁵⁴ $A - 5B \equiv U - 3J_H^b$. This leads to $r_1^b = \frac{1}{1-3J_H^b/U}$.

(ii) The low spin state 1T_1 on copper sites (middle bottom panel of Fig. 4) which involves $d^2 = b^1a^1$ or-

bital configuration and with energy in terms of Racah parameters⁵⁴ $A + B + 2C \equiv U - J_H^b$. This leads to $r_2^b = \frac{1}{1-J_H^b/U}$.

(iii) The high spin state 3T_1 on oxygen sites (middle top panel of Fig. 3; note that due to the equivalence between the t_{2g}^2 and p^2 configuration⁵⁴ we can label the multiplet states on the p shell by those known from the t_{2g} sector) which involves $p^2 = x^1z^1$ orbital configuration and with energy in terms of Racah parameters⁵⁴ $A_o - 5B_o \equiv U_p - 3J_H^p$ (where o denotes the fact that the Racah parameters are for oxygen sites). This leads to $R_1^b = \frac{2U}{\Delta_x + \Delta_z + U_p(1-3J_H^p/U_p)}$.

(iv) The low spin state 1T_2 on oxygen sites (middle top panel of Fig. 4) which involves $p^2 = x^1z^1$ orbital configuration and with energy in terms of Racah parameters⁵⁴ $A_o + B_o + 2C_o \equiv U_p - J_H^p$. This leads to $R_2^b = \frac{2U}{\Delta_x + \Delta_z + U_p(1-J_H^p/U_p)}$.

D. Spin-orbital superexchange for c orbital: $\bar{\mathcal{H}}_c$

If along a bond there is one hole in the c orbital (due to e.g. an orbital excitation created in RIXS) and another one in the a orbital, then using the perturbation theory to fourth order in t_n we obtain (cf. Figs 3-4 showing an analogous situation in the case of the orbital superexchange between the b and a orbitals):

$$\begin{aligned} \bar{\mathcal{H}}_c = & \sum_i \left(\mathbf{S}_i \cdot \mathbf{S}_{i+1} + \frac{3}{4} \right) \left[\left(R_1^c J_{12}^c + r_1^c \frac{J_1 + J_2^c}{2} \right) \right. \\ & \left. \left(\tau_i^z \tau_{i+1}^z - \frac{1}{4} \right) + \frac{R_1^c + r_1^c}{2} J_{12}^c (\tau_i^+ \tau_{i+1}^- + \tau_i^- \tau_{i+1}^+) \right] \\ & + \sum_i \left(\frac{1}{4} - \mathbf{S}_i \cdot \mathbf{S}_{i+1} \right) \left[\left(R_2^c J_{12}^c + r_2^c \frac{J_1 + J_2^c}{2} \right) \right. \\ & \left. \left(\tau_i^z \tau_{i+1}^z - \frac{1}{4} \right) - \frac{R_2^c + r_2^c}{2} J_{12}^c (\tau_i^+ \tau_{i+1}^- + \tau_i^- \tau_{i+1}^+) \right], \end{aligned} \quad (19)$$

where the superexchange constants are J_1 [cf. Eq. (14)] and

$$J_2^c = \left(\frac{2\bar{t}_\pi^2}{\Delta_y + V_{dp}} \right)^2 \frac{1}{U}, \quad (20)$$

with $\bar{t}_\pi = \lambda_c t_\pi$ (see Appendix A for origin of the factor λ_c) and

$$J_{12}^c = \frac{(2\bar{t}_\pi \bar{t}_\sigma)^2}{(\Delta_y + V_{dp})(\Delta_x + V_{dp})} \frac{1}{U}. \quad (21)$$

Similarly to the b orbital case discussed above, the complex structure of Hamiltonian (19) is a consequence of the fact that the proper derivation of such low energy model has to include the superexchange processes with four distinct intermediate states:

(i) The high spin state 3T_1 on copper sites which involves $d^2 = c^1a^1$ orbital configuration and with energy in terms of Racah parameters⁵⁴ $A + 4B \equiv U - 3J_H^c$. This leads to $r_1^c = \frac{1}{1-3J_H^c/U}$.

(ii) The low spin state 1T_1 on copper sites which involves $d^2 = c^1a^1$ orbital configuration and with energy in terms of Racah parameters⁵⁴ $A + 4B + 2C \equiv U - J_H^c$. This leads to $r_2^c = \frac{1}{1-J_H^c/U}$.

(iii) The high spin state 3T_1 on oxygen sites which involves $p^2 = x^1y^1$ orbital configuration and with energy in terms of Racah parameters⁵⁴ $A_o - 5B_o \equiv U_p - 3J_H^p$. This leads to $R_1^c = \frac{2U}{\Delta_x + \Delta_y + U_p(1-3J_H^p/U_p)}$.

(iv) The low spin state 1T_2 on oxygen sites which involves $p^2 = x^1y^1$ orbital configuration and with energy in terms of Racah parameters⁵⁴ $A_o + B_o + 2C_o \equiv U_p - J_H^p$. This leads to $R_2^c = \frac{2U}{\Delta_x + \Delta_y + U_p(1-J_H^p/U_p)}$.

E. Remarks on the derivation and parameters

Firstly, we would like to remark that the physics of superexchange interactions is very similar in both ‘orbital exchange’ cases discussed above [cf. Eq. (16) and Eq. (19)]. Thus, the main (quantitative) difference between these two cases originates in slightly renormalized model parameters. Secondly, we should comment on the superexchange paths which, due to their small relative contribution to the low energy Hamiltonian, are neglected in the above derivation:

(i) There is a finite probability that e.g. the c^1a^1 (i.e. $t_{2g}^1 e_g^1$) configuration in the intermediate state 3T_1 decays into a t_{2g}^2 configuration. However, such process can be neglected, since this means that in the final state of the superexchange process we would then be left with a transition to a higher energy sector: starting from the initial state with one hole in a t_{2g} configuration we would end with two holes in the t_{2g} configuration in the final state of the superexchange process and this would cost the energy $\sim \bar{\varepsilon}_b$ or $\sim \bar{\varepsilon}_c$; the latter energies are typically much larger than the scales of the superexchange interactions.

(ii) We also neglect intermediate states of the kind 1A_1 or 1E or 3A_2 , since they all require transitions to the higher energy sector $\sim \bar{\varepsilon}_b$ or $\sim \bar{\varepsilon}_c$.

(iii) Finally, from the above structure one can see that it is impossible to have a ‘mixing’ between the t_{2g} orbital excitations, i.e. to have transitions between the states with e.g. $a_i^1 c_{i+1}^1$ configuration and e.g. $b_i^1 a_{i+1}^1$ configuration – this is due to: (a) the flavor-conserving hoppings between the t_{2g} orbitals, and (b) no on-site hopping [cf. Eq. (1)] allowing for a transition from c^1a^1 to b^1a^1 state, cf. Table A26 from Ref. 54.

Finally, let us note that all of the parameters of the spin-orbital model directly follow from the charge transfer model parameters. Their values are shown in Table I.

IV. ORBITON SPECTRAL FUNCTIONS

Our main purpose is to calculate the orbiton dispersion, which follows from the two orbiton spectral functions

$$A_b(k, \omega) \equiv \frac{1}{\pi} \lim_{\eta \rightarrow 0} \Im \langle 0 | \sum_{j\sigma} e^{ikj} f_{ja\sigma}^\dagger f_{jb\sigma} \times \frac{1}{\omega + E_0 - \mathcal{H} - i\eta} \sum_{j\sigma} e^{ikj} f_{jb\sigma}^\dagger f_{ja\sigma} | 0 \rangle, \quad (22)$$

and

$$A_c(k, \omega) \equiv \frac{1}{\pi} \lim_{\eta \rightarrow 0} \Im \langle 0 | \sum_{j\sigma} e^{ikj} f_{ja\sigma}^\dagger f_{jc\sigma} \times \frac{1}{\omega + E_0 - \mathcal{H} - i\eta} \sum_{j\sigma} e^{ikj} f_{jc\sigma}^\dagger f_{ja\sigma} | 0 \rangle, \quad (23)$$

where $|0\rangle$ is the ground state of the charge transfer Hamiltonian \mathcal{H} , Eq. (1), with energy E_0 .

In what follows we will concentrate on the low energy version of the charge transfer Hamiltonian, i.e. the spin-orbital Hamiltonian Eq. (6). Thus, we express the above formulae for orbiton spectral functions in terms of the orbital pseudospin operators acting in the restricted Hilbert space of the spin-orbital Hamiltonian without double occupancies⁶⁰:

$$A_b(k, \omega) = \frac{1}{\pi} \lim_{\eta \rightarrow 0} \Im \langle \bar{0} | \sigma_k \frac{1}{\omega + E_{\bar{0}} - \mathcal{H} - i\eta} \sigma_k^\dagger | \bar{0} \rangle, \quad (24)$$

$$A_c(k, \omega) = \frac{1}{\pi} \lim_{\eta \rightarrow 0} \Im \langle \bar{0} | \tau_k \frac{1}{\omega + E_{\bar{0}} - \mathcal{H} - i\eta} \tau_k^\dagger | \bar{0} \rangle, \quad (25)$$

where $|\bar{0}\rangle$ is the ground state of the spin-orbital Hamiltonian \mathcal{H} with energy $E_{\bar{0}}$. It is now easy to verify that, for the realistic regime of parameters defined in Table I, the ground state is insulating, ferroorbital (FO) i.e. only orbital a is occupied, and antiferromagnetic (AF) (due to its 1D nature and lack of long range order called ‘quantum’ AF in what follows). This is because the energy cost of populating b or c orbital states $\bar{\epsilon}_b$ and $\bar{\epsilon}_c$ is much larger than hopping t_n (cf. Table I). Thus, it is only the spin Heisenberg Hamiltonian \mathcal{H}_a which dictates what is the spin ground state (which is always AF for any positive J_1 and R , cf. Table I).

In the following subsections we calculate the orbiton spectral functions, Eqs. (24)-(25): firstly by mapping them onto the spectral functions of the effective t - J model problems and then by solving these simplified problems numerically. While this method is not entirely exact, it gives far better approximation of the actual spectral function than the commonly used linear orbital wave approximation, cf. part 1 and part 3 of Appendix B.

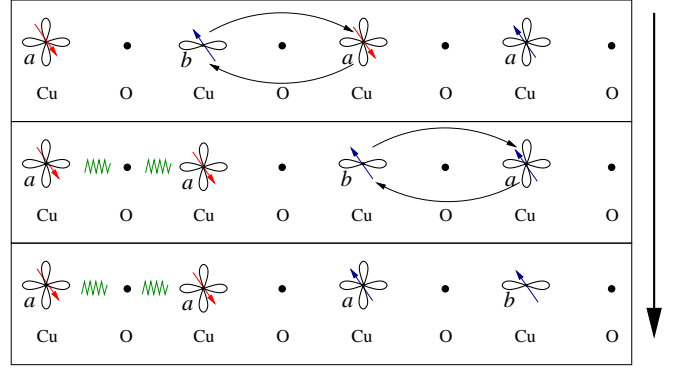


FIG. 5: (Color online) Schematic view of the propagation of the orbiton in the spin-orbital separation scenario: the orbiton hops to the neighboring site (top panel) and initially excites a single spinon (middle panel) but then separates from the spinon and can freely travel in the 1D AF (bottom panel).

A. Mapping onto the effective t - J models

Mapping for the b orbiton case.— To address the issues mentioned above, we rewrite Eq. (24) in the following way:

$$A_b(k, \omega) = \frac{1}{\pi} \lim_{\eta \rightarrow 0} \Im \langle \bar{0} | \sum_j e^{ikj} \sigma_j \left(\frac{1}{2} - S_j^z \right) \times \frac{1}{\omega + E_{\bar{0}} - \mathcal{H} - i\eta} \sum_j e^{ikj} \sigma_j^\dagger \left(\frac{1}{2} - S_j^z \right) | \bar{0} \rangle + \frac{1}{\pi} \lim_{\eta \rightarrow 0} \Im \langle \bar{0} | \sum_j e^{ikj} \sigma_j \left(\frac{1}{2} + S_j^z \right) \times \frac{1}{\omega + E_{\bar{0}} - \mathcal{H} - i\eta} \sum_j e^{ikj} \sigma_j^\dagger \left(\frac{1}{2} + S_j^z \right) | \bar{0} \rangle. \quad (26)$$

Here we used an approximation that the spectral function for an orbiton is only nonzero when the spin of the hole in the excited orbital is conserved [i.e. we assumed that the spectral functions for orbiton, which contains the ‘cross terms’ of the kind $\propto (\frac{1}{2} + S_j^z)(\frac{1}{2} - S_j^z)$, can be neglected]. In fact, this approximation amounts to neglecting the process which describes orbiton propagation with an additional spin flip, see part 3 of Appendix B for justification that such process has relatively small amplitude and can be neglected. Furthermore, due to the SU(2) spin invariance of both the ground state $|\bar{0}\rangle$ and of the Hamiltonian \mathcal{H} , the two contributions to the spectral function [as written on the right hand side of Eq. (26)] are equal, i.e. we can write

$$A_b(k, \omega) = \frac{2}{\pi} \lim_{\eta \rightarrow 0} \Im \langle \bar{0} | \sum_j e^{ikj} \sigma_j \left(\frac{1}{2} - S_j^z \right) \times \frac{1}{\omega + E_{\bar{0}} - \mathcal{H} - i\eta} \sum_j e^{ikj} \sigma_j^\dagger \left(\frac{1}{2} - S_j^z \right) | \bar{0} \rangle. \quad (27)$$

Next we introduce fermions (to be called spinons) α through the Jordan-Wigner (JW) transformation for

spins and fermions β (to be called pseudospinons) through the JW transformation for pseudospins, cf. Ref. 49. We define

$$\begin{aligned} S_j^+ &= \exp\left(-i\pi \sum_{n=1,\dots,j-1} Q_n\right) \alpha_j^\dagger, \\ S_j^- &= \alpha_j \exp\left(i\pi \sum_{n=1,\dots,j-1} Q_n\right), \\ S_j^z &= n_{j\alpha} - \frac{1}{2}. \end{aligned} \quad (28)$$

where $Q_n = \alpha_n^\dagger \alpha_n$ and α_n are fermions. Besides, we define the orbital fermionic operators β as:

$$\begin{aligned} \sigma_j^+ &= \exp\left(-i\pi \sum_{n=1,\dots,j-1} \bar{Q}_n\right) \beta_j^\dagger, \\ \sigma_j^- &= \beta_j \exp\left(i\pi \sum_{n=1,\dots,j-1} \bar{Q}_n\right), \\ \sigma_j^z &= n_{j\beta} - \frac{1}{2}, \end{aligned} \quad (29)$$

where $\bar{Q}_n = \beta_n^\dagger \beta_n$ and β_n are fermions.

It turns out that when calculating the orbiton spectral function Eq. (27) with spins and pseudospins expressed in terms of the JW fermions following the above transformation, a pseudospinon and spinon are not present on the same site, cf. Ref. 49. In other words, we have a constraint

$$\forall_i (\beta_i^\dagger \beta_i + \alpha_i^\dagger \alpha_i) \leq 1, \quad (30)$$

since otherwise the right hand side of the spectral function in Eq. (27) is zero because $\sigma_j^\dagger(\frac{1}{2} - S_j^z) = \beta_j^\dagger(1 - n_{j\alpha})$. The physical understanding of this phenomenon is as follows: suppose one promotes a hole with spin down to the b orbital at site i , which means that we have no pseudospinon and spinon at this site. Now, this pseudospinon can move only via such processes which do not flip the spin of the hole in the b orbital, i.e. we prohibit creating spinon and pseudospinon at the same site [cf. part 3 of Appendix B].

Altogether this means that while rewriting the low energy Hamiltonian Eqs. (10), (11) and (16) in terms of fermions α and β we can skip all the terms which contain the pseudospinon and spinon at the same site. We arrive at the following Hamiltonian

$$H_{\text{JW}}^{ab} \equiv H_{\text{JW}}^0 + H_{\text{JW}}^a + H_{\text{JW}}^b \quad (31)$$

with

$$H_{\text{JW}}^0 = \bar{\varepsilon}_b \sum_i \beta_i^\dagger \beta_i, \quad (32)$$

$$\begin{aligned} H_{\text{JW}}^a &= J_1(1+R) \sum_i (1 - n_{i\beta}) \left[\frac{1}{2} (\alpha_i^\dagger \alpha_{i+1} + h.c.) \right. \\ &\quad \left. - \frac{1}{2} n_{i\alpha} - \frac{1}{2} n_{i+1\alpha} + n_{i\alpha} n_{i+1\alpha} \right] (1 - n_{i+1\beta}), \end{aligned} \quad (33)$$

(with the pseudospinon operators originating in the projection operators $\mathcal{P}_{i,i+1}$) and

$$\begin{aligned} H_{\text{JW}}^b &= -\frac{1}{4} (R_1^b + r_1^b + R_2^b + r_2^b) J_{12}^b \sum_i (\alpha_i^\dagger \beta_i \beta_{i+1}^\dagger \alpha_{i+1} + h.c.) \\ &\quad - \frac{1}{2} (R_1^b + r_1^b) J_{12}^b \sum_i (\beta_i \beta_{i+1}^\dagger + h.c.) \\ &\quad - \left(R_1^b J_{12}^b + r_1^b \frac{J_1 + J_2^b}{2} \right) \sum_i \beta_i^\dagger \beta_i, \end{aligned} \quad (34)$$

where in addition we assumed that only one pseudospinon in the bulk is present (which corresponds to the FO ground state with one orbital excitation) and we skipped the terms $n_{i\alpha} n_{i+1\beta} + n_{i+1\alpha} n_{i\beta}$, as for realistic value of J_H^b and J_P^b (cf. Table I) they are of the order of 10%-20% of the value of the hopping t_b [see Eq. (37) below and Table I].

Next, we perform a transformation that connects the above derived Hamiltonian with the effective t - J model. Thus, we introduce the auxiliary fermions $\tilde{p}_{i\sigma}$ acting in a Hilbert space without double occupancies [we have checked that the operators $\tilde{p}_{i\sigma}$ fulfill the appropriate commutation rules (cf. Ref. 61)]:

$$\begin{aligned} \tilde{p}_{j\uparrow} &= \beta_j^\dagger, \\ \tilde{p}_{j\downarrow} &= \beta_j^\dagger \alpha_j \exp\left(i\pi \sum_{n=1,\dots,j-1} Q_n\right), \end{aligned} \quad (35)$$

where again $Q_n = \alpha_n^\dagger \alpha_n$. Besides, we introduce back spin operators \mathbf{S} following Eq. (28). Thus, we obtain

$$\begin{aligned} H_{t-J}^{ab} &\equiv H_{t-J}^0 + H_{t-J}^a + H_{t-J}^b = -t_b \sum_{j,\sigma} (\tilde{p}_{j\sigma}^\dagger \tilde{p}_{j+1\sigma} + h.c.) \\ &\quad + J \sum_j \left(\mathbf{S}_j \mathbf{S}_{j+1} - \frac{1}{4} \tilde{n}_j \tilde{n}_{j+1} \right) - E_b^h \sum_j \tilde{n}_j, \end{aligned} \quad (36)$$

where the parameters are defined as

$$t_b \equiv \frac{1}{8} (3R_1^b + R_2^b + 3r_1^b + r_2^b) J_{12}^b, \quad (37)$$

$$J \equiv J_1(1+R), \quad (38)$$

$$E_b^h \equiv \bar{\varepsilon}_b - (R_1^b J_{12}^b + r_1^b \frac{J_1 + J_2^b}{2}), \quad (39)$$

and we furthermore neglected the difference between $t_{b\downarrow} \equiv \frac{1}{4} (R_1^b + R_2^b + r_1^b + r_2^b) J_{12}^b$ and $t_{b\uparrow} \equiv \frac{1}{2} (R_1^b + r_1^b) J_{12}^b$ hopping element. Note, however that: (i) this difference is of ca. 10 % for realistic parameters from Table I and therefore can be neglected to simplify the calculations, (ii) keeping this difference while at the same time neglecting the possibility of orbiton propagation with an additional spin flip (the so-called B1 process in part 3 of Appendix B) violates the SU(2) spin symmetry of the original Hamiltonian, and finally (iii) we have verified that *including* this difference not only does not lead to

qualitatively different RIXS cross section but also the quantitative changes are negligible.

As the last step we express also the b orbiton spectral function, Eq. (27), in the t - J model language. Using the same transformations as for the Hamiltonian above we obtain

$$A_b(k, \omega) = \frac{2}{\pi} \lim_{\eta \rightarrow 0} \Im \langle \Phi | \tilde{p}_{k\uparrow}^\dagger \frac{1}{\omega + E_\Phi - H_{t-J}^{ab} - i\eta} \tilde{p}_{k\uparrow} | \Phi \rangle, \quad (40)$$

here $|\Phi\rangle$ is the ground state of H_{t-J}^{ab} at half-filling with energy E_Φ (i.e. is a 1D quantum AF). Let us note that the t - J model spectral function does not depend on the spin σ of the fermion $\tilde{p}_{k\sigma}$ which is consistent with the fact that the choice of spin σ in Eq. (35) was arbitrary.

Mapping for the c orbiton case.— Following the same steps as for the b orbiton spectral function we obtain the effective t - J Hamiltonian

$$\begin{aligned} H_{t-J}^{ac} \equiv & H_{t-J}^0 + H_{t-J}^a + H_{t-J}^c = -t_c \sum_{j,\sigma} (\tilde{p}_{j\sigma}^\dagger \tilde{p}_{j+1\sigma} + h.c.) \\ & + J \sum_j \left(\mathbf{S}_j \mathbf{S}_{j+1} - \frac{1}{4} \tilde{n}_j \tilde{n}_{j+1} \right) - E_c^h \sum_j \tilde{n}_j, \end{aligned} \quad (41)$$

where the parameters are defined as

$$t_c \equiv \frac{1}{8} (3R_1^c + R_2^c + 3r_1^c + r_2^c) J_{12}^c, \quad (42)$$

$$J \equiv J_1 (1 + R), \quad (43)$$

$$E_c^h \equiv \bar{\varepsilon}_c - (R_1^c J_{12}^b + r_1^c \frac{J_1 + J_2}{2}). \quad (44)$$

The spectral function is then defined as

$$A_c(k, \omega) = \frac{2}{\pi} \lim_{\eta \rightarrow 0} \Im \langle \Phi | \tilde{p}_{k\uparrow}^\dagger \frac{1}{\omega + E_\Phi - H_{t-J}^{ac} - i\eta} \tilde{p}_{k\uparrow} | \Phi \rangle. \quad (45)$$

Parameters after the mapping.— As shown above, the parameters t_b , t_c , and J in the effective t - J model are expressed in terms of the spin-orbital model parameters from the middle column of Table I. Thus they can be easily calculated and their precise values are given in the right column of Table I. On the other hand, while the energies of the on-site orbital excitations E_b^h and E_c^h also follow from these parameters, in order to stay in line with Ref. 22, we directly estimate them following the *ab-initio* quantum chemistry calculations on three CuO_3 plaquettes in Sr_2CuO_3 , cf. Ref. 22. Note that these *ab-initio* calculations are performed for ferromagnetic chain and hence they are ‘well-suited’ to our needs, since we have $E_b^h \simeq E_b$ ($E_c^h \simeq E_c$) where E_b (E_c) is defined as the on-site cost of a b (c) orbital excitation in a ferromagnetic environment. Let us note that both methods lead to rather similar results, i.e. estimating E_b^h and E_c^h directly from the spin-orbital model parameters given in Table I would lead to similar values as the reported here *ab-initio* values.

B. Spin-orbital separation and numerical results

Altogether, we see that we managed to map the spin-orbital problem with an FO and AF ground state and one excitation in the b or c orbital onto an effective t - J model with an AF ground state and one empty site (‘hole’) without a spin (cf. Ref. 49 and also Ref. 62 which also shows a mapping of a spin-like problem onto an effective t - J model). As the latter problem is well-known⁶³, even before calculating the spectral function, we can draw an interesting conclusion: The t - J model spectral function at half filling, when calculated in 1D, describes a phenomenon called spin-charge separation. This means that the ‘hole’ in the 1D AF separates into an independent holon, which carries charge quantum number, and spinon which carries spin quantum number. Thus, also the here discussed spin-orbital problem shows such separation phenomenon – to be called *spin-orbital separation*. In fact, this can also be understood by looking at the cartoon picture in Fig. 5: (i) the orbiton moves in such a way that the spin of the hole in this excited orbital is conserved, (ii) this motion introduces a single defect in the AF ground state (spinon), and (iii) the created spinon and the ‘pure’ orbiton (holon in the t - J model language) can move independently and completely separate⁴⁹.

Nevertheless, i.e. despite the fact that the t - J model spectral function is well-known, we calculate the spectral functions Eq. (40) and Eq. (45) using the Lanczos exact diagonalization on a 28-site chain separately for each orbiton case. The spectral function for the b orbiton $[A_b(k, \omega)]$ and c orbiton case $[A_c(k, \omega)]$ is shown in Fig. 6. The spectrum for each orbiton case consists of a lower lying orbiton branch with dispersion $\propto t_b$ (or $\propto t_c$), period π , and mixed spinon-orbiton excitation bounded from above by the edge $\propto \sqrt{J^2 + 4t^2 + 4tJ \cos k}$ with $t \equiv t_b$ or $t \equiv t_c$ depending on the orbiton under consideration, cf. Ref. 49. Note that this spectrum is quantitatively (but not qualitatively) different than the ‘usual’ spin-charge separation. The latter is ‘normally’ calculated for the case $J < t$ (whereas in ‘our’ spin-orbital case $J > t$ in the effective t - J model)⁴⁹.

V. RIXS CROSS SECTION

In this section we calculate the RIXS spectra of the orbital excitations in Sr_2CuO_3 . As it is well-established^{13,14,20} that RIXS is an excellent probe of orbital excitations, the calculations are rather straightforward provided the orbiton spectral function is known.

Following References 6,15, using the dipole approximation and the so-called fast collision approximation^{64,65}, the RIXS cross section for orbital excitations at the Cu^{2+}

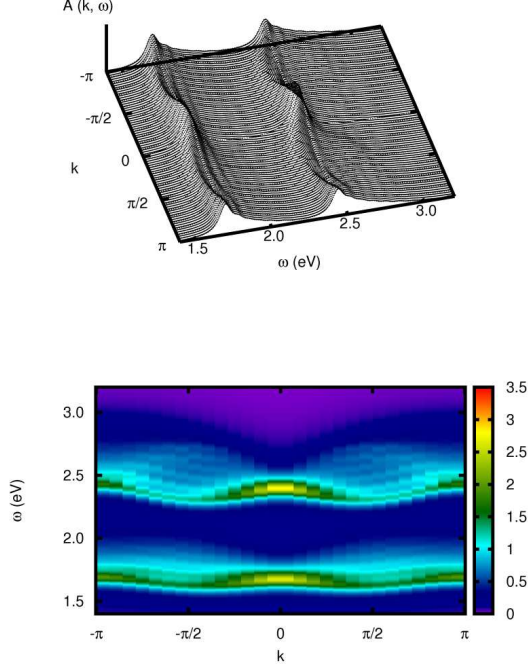


FIG. 6: (Color online) Spectral function $A_b(k, \omega) + A_c(k, \omega)$ as a function of momentum k and energy transfer ω in the spin-orbital scenario and calculated using Lanczos exact diagonalization on a 28 site chain. Results for broadening $\eta = 0.05$ eV which gives FWHM = 0.1 eV, i.e. the experimental resolution of RIXS in Sr_2CuO_3 ²².

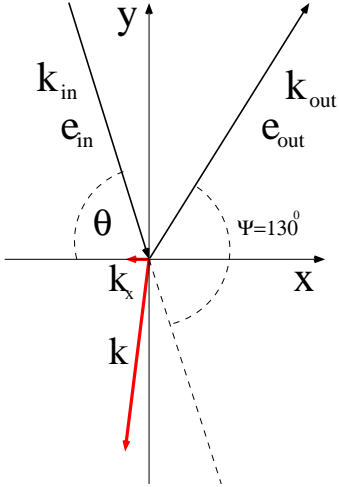


FIG. 7: (Color online) Geometry of the RIXS experiment performed on Sr_2CuO_3 and presented in Ref. 22 shown here for the $\Psi = 130^\circ$ scattering angle. The momentum transfer k_x is denoted as k in the main text.

L edge in the 1D copper oxygen chain reads

$$I(k, \omega; \mathbf{e}) = \frac{1}{\pi} \lim_{\eta \rightarrow 0} \Im \langle 0 | T_S^\dagger(k, \mathbf{e}) \times \frac{1}{\omega + E_0 - \mathcal{H} - i\eta} T_S(k, \mathbf{e}) | 0 \rangle, \quad (46)$$

where $\omega \equiv \omega_{out} - \omega_{in}$ is the photon energy loss, $\mathbf{k} \equiv \mathbf{k}_{in} - \mathbf{k}_{out}$ is the photon momentum loss (with $k \equiv k_x = \mathbf{k} \cdot \hat{\mathbf{x}}$ being the momentum loss along the x direction of the copper oxygen chain in the studied case of Sr_2CuO_3 , cf. Fig. 1), and $|0\rangle$ is the ground state of Hamiltonian \mathcal{H} with energy E_0 , see Eq. (1) and cf. Eqs. (22)-(23). Finally, $T_S(k, \mathbf{e})$ is the RIXS scattering operator, which depends on the incoming and outgoing photon polarization $\mathbf{e} = \mathbf{e}_{in} \mathbf{e}_{out}^\dagger$ in the RIXS experiment. It reads^{6,15,65}

$$T_S = T_b + T_c + T_d + T_e = \sum_{j, \sigma, \sigma'} e^{ikj} [B_{\sigma, \sigma'}(\mathbf{e}) f_{jb\sigma}^\dagger f_{ja\sigma'} + C_{\sigma, \sigma'}(\mathbf{e}) f_{jc\sigma}^\dagger f_{ja\sigma'} + D_{\sigma, \sigma'}(\mathbf{e}) f_{jd\sigma}^\dagger f_{ja\sigma'} + E_{\sigma, \sigma'}(\mathbf{e}) f_{je\sigma}^\dagger f_{ja\sigma'}]. \quad (47)$$

Here: (i) orbital $d = 3d_{yz}$, orbital $e = 3d_{3z^2-r^2}$, and the other orbitals are defined as in Eq. (1), (ii) operator $f_{j\alpha\sigma}^\dagger$ and $f_{j\alpha\sigma}$ is defined as in Eq. (1) with $\alpha \in \{a, b, c, d, e\}$, (iii) $B_{\sigma, \sigma'}$, $C_{\sigma, \sigma'}$, $D_{\sigma, \sigma'}$, and $E_{\sigma, \sigma'}$ are complex numbers which define the so-called RIXS matrix elements. The latter ones can be easily calculated in the fast collision approximation, see immediately below.

A. RIXS matrix elements

To calculate the above defined RIXS matrix elements in the fast collision approximation, and to be able to compare the obtained results with the experimental ones reported in Ref. 22, we assume that: (i) the incoming energy of the photon is tuned to the copper L_3 edge, i.e. $\omega_{in} \simeq 930$ eV, and thus the wavevector of the incoming photon is $k_{in} \simeq 0.471/\text{\AA}$, (ii) the wavevector at the edge of the Brillouin zone along the x direction in Sr_2CuO_3 is $0.8051/\text{\AA}$ as the lattice constant is⁵² 3.91\AA , (iii) in the ionic picture the ground state configuration at the copper site is $3d^9$, (iv) the relatively small spin-orbit coupling in the $3d$ shell can be neglected, (v) the incoming polarization vector \mathbf{e}_{in} is parallel to the scattering plane and the outgoing polarization vector is not measured, cf. Fig. 7, (vi) the scattering plane is the xy plane, i.e. the one in which the copper oxygen chain lies (which runs along the x direction, see Fig. 1), cf. Fig. 7, and (vii) the angle between the outgoing and the incoming photon momentum is either $\psi = 90^\circ$ or $\psi = 130^\circ$, cf. Fig. 7. The latter defines the two scattering geometries used in the RIXS experiment reported in Ref. 22.

Next, we calculate the RIXS matrix elements in three steps:

Firstly, following *inter alia* Ref. 15, we express the matrix elements in terms of the different components of

the incoming and outgoing polarization vectors and the spin operator. These expressions can be easily obtained from Fig. 1 of Ref. 15 and hence we do not write them here.

Secondly, we express the incoming and outgoing polarization vectors in terms of the angle θ measured between the momentum of the incoming photon and the x chain direction, cf. Fig. 7 (note the convention that if $k < 0$, then $\theta \rightarrow 0$): (i) the vector of the incoming polarization of the photon in terms of the angle θ is $\mathbf{e}_{in} = [\sin \theta, \cos \theta, 0]$, (ii) the vector of the outgoing polarization of the photon in terms of the angle θ is $\mathbf{e}_{out} = [-\cos \theta, \sin \theta, 0]$ for π polarization and $\mathbf{e}_{out} = [0, 0, 1]$ for σ polarization in the $\psi = 90^\circ$ geometry, and (iii) the vector of the outgoing polarization of the photon in terms of the angle θ is $\mathbf{e}_{out} = [-\cos(\theta - 40^\circ), \sin(\theta - 40^\circ), 0]$ for π polarization and $\mathbf{e}_{out} = [0, 0, 1]$ for σ polarization in the $\psi = 130^\circ$ geometry.

Thirdly, we express the angle θ in terms of the transferred momentum k along the x direction: (i) for $\psi = 90^\circ$ geometry the transferred momentum as a function of angle $\theta \in (0^\circ, 90^\circ)$ is $k \simeq 0.58\sqrt{2}\pi \sin(\theta - 45^\circ)$ where the distance between the copper sites along the chain is assumed to be equal to unity, and (ii) for $\psi = 130^\circ$ the angle changes as $\theta \in (0^\circ, 130^\circ)$ and $k \simeq 1.07\pi \sin(\theta - 65^\circ)$.

Altogether, this shows how to calculate the RIXS matrix elements for orbital excitations and that the latter effectively becomes a function of transferred momentum k and energy ω . Therefore, in what follows, we simplify notation and write $I(k, \omega; \mathbf{e}) \rightarrow I(k, \omega)$.

B. Numerical results

We first express the RIXS cross section for the b and c orbital excitations in terms of the previously calculated (see Sec. IV) b and c orbiton spectral functions. In order to do so, we use the fact that according to the analysis in Sec. IV A the spin of the hole in the excited orbital does not change during the orbiton propagation process. Thus, for e.g. only the b part of the RIXS cross section we can write:

$$\begin{aligned}
 I_b(k, \omega) &= \frac{1}{\pi} \lim_{\eta \rightarrow 0} \Im \langle 0 | \sum_{\sigma_1, j} B_{\sigma_1, \uparrow}^* e^{ikj} f_{ja\sigma_1}^\dagger f_{jc\uparrow} \\
 &\quad \times \frac{1}{\omega + E_0 - \mathcal{H} - i\eta} \sum_{\sigma_2, j} B_{\uparrow, \sigma_2} e^{ikj} f_{jc\uparrow}^\dagger f_{ja\sigma_2} | 0 \rangle \\
 &\quad + \frac{1}{\pi} \lim_{\eta \rightarrow 0} \Im \langle 0 | \sum_{\sigma_1, j} B_{\sigma_1, \downarrow}^* e^{ikj} f_{ja\sigma_1}^\dagger f_{jc\downarrow} \\
 &\quad \times \frac{1}{\omega + E_0 - \mathcal{H} - i\eta} \sum_{\sigma_2, j} B_{\downarrow, \sigma_2} e^{ikj} f_{jc\downarrow}^\dagger f_{ja\sigma_2} | 0 \rangle.
 \end{aligned} \tag{48}$$

Next, we can employ the transformations used in Sec. III and IV A to map the above problem first onto a spin-orbital model and then onto an effective t - J model prob-

lem. We obtain then:

$$\begin{aligned}
 I_b(k, \omega) &= \frac{1}{\pi} \lim_{\eta \rightarrow 0} \Im \langle \Phi | (B_{\uparrow, \uparrow}^* \tilde{p}_{k\uparrow}^\dagger + B_{\uparrow, \downarrow}^* \tilde{p}_{k\downarrow}^\dagger) \\
 &\quad \frac{1}{\omega + E_\Phi - H_{t-J}^{ab} - i\eta} (B_{\uparrow, \uparrow} \tilde{p}_{k\uparrow} + B_{\uparrow, \downarrow} \tilde{p}_{k\downarrow}) | \Phi \rangle \\
 &\quad + \frac{1}{\pi} \lim_{\eta \rightarrow 0} \Im \langle \Phi | (B_{\downarrow, \downarrow}^* \tilde{p}_{k\uparrow}^\dagger + B_{\downarrow, \uparrow}^* \tilde{p}_{k\downarrow}^\dagger) \\
 &\quad \frac{1}{\omega + E_\Phi - H_{t-J}^{ab} - i\eta} (B_{\downarrow, \downarrow} \tilde{p}_{k\uparrow} + B_{\downarrow, \uparrow} \tilde{p}_{k\downarrow}) | \Phi \rangle.
 \end{aligned} \tag{49}$$

Finally, the ‘interference’ terms in the above equation cancel due to the identity relations between the RIXS matrix elements

$$B_{\uparrow, \uparrow} B_{\downarrow, \uparrow}^* = -B_{\downarrow, \downarrow}^* B_{\uparrow, \downarrow} \tag{50}$$

which leads to:

$$I_b(k, \omega) = (|B_{\uparrow, \uparrow}|^2 + |B_{\downarrow, \uparrow}|^2) A_b(k, \omega), \tag{51}$$

where we used that (see Sec. IV A)

$$\begin{aligned}
 A_b(k, \omega) &= \frac{1}{\pi} \lim_{\eta \rightarrow 0} \Im \langle \Phi | \tilde{p}_{k\uparrow}^\dagger \frac{1}{\omega + E_\Phi - H_{t-J}^{ab} - i\eta} \tilde{p}_{k\uparrow} | \Phi \rangle \\
 &= \frac{1}{\pi} \lim_{\eta \rightarrow 0} \Im \langle \Phi | \tilde{p}_{k\downarrow}^\dagger \frac{1}{\omega + E_\Phi - H_{t-J}^{ab} - i\eta} \tilde{p}_{k\downarrow} | \Phi \rangle
 \end{aligned} \tag{52}$$

and $A_b(k, \omega)$ was calculated in Sec. IV. Employing the same transformation for the c orbiton, we obtain $I_c(k, \omega) = (|C_{\uparrow, \uparrow}|^2 + |C_{\downarrow, \uparrow}|^2) A_c(k, \omega)$ with $A_c(k, \omega)$ also calculated in Sec. IV.

Secondly, to complete the RIXS calculations we also have to add the spectra for the dispersionless excitations to the d and e orbitals. As this task is straightforward, cf. Appendix C, we obtain for the total RIXS cross section

$$\begin{aligned}
 I(k, \omega) &= (|B_{\uparrow, \uparrow}|^2 + |B_{\downarrow, \uparrow}|^2) A_b(k, \omega) \\
 &\quad + (|C_{\uparrow, \uparrow}|^2 + |C_{\downarrow, \uparrow}|^2) A_c(k, \omega) \\
 &\quad + (|D_{\uparrow, \uparrow}|^2 + |D_{\uparrow, \downarrow}|^2) \delta(\omega - E_d - E_{AF}) \\
 &\quad + (|E_{\uparrow, \uparrow}|^2 + |E_{\uparrow, \downarrow}|^2) \delta(\omega - E_e - E_{AF}).
 \end{aligned} \tag{53}$$

Note that the values of the on-site orbital energies of the dispersionless orbital excitations, E_d and E_e , are obtained from the quantum chemistry *ab-initio* calculations for a ferromagnetic chain consisting of three CuO_3 plaquettes, cf. Table I. Since these values are given for a ferromagnetic chain, we have to add the energy cost of a single spin flip (E_{AF}), which is also calculated using the same *ab-initio* method, cf. Table I for its precise value.

Comparison with the experiment.— The RIXS cross section calculated according to Eq. (53) is shown in Fig. 8. Comparing this theoretical spectrum against the experimental one shown in Fig. 4(a) in Ref. 22 [for the case of the scattering angle $\Psi = 130^\circ$; a similar agreement is obtained for the unpublished RIXS experimental results⁶⁶ for the scattering angle $\Psi = 90^\circ$] we note the following similarities between the two:

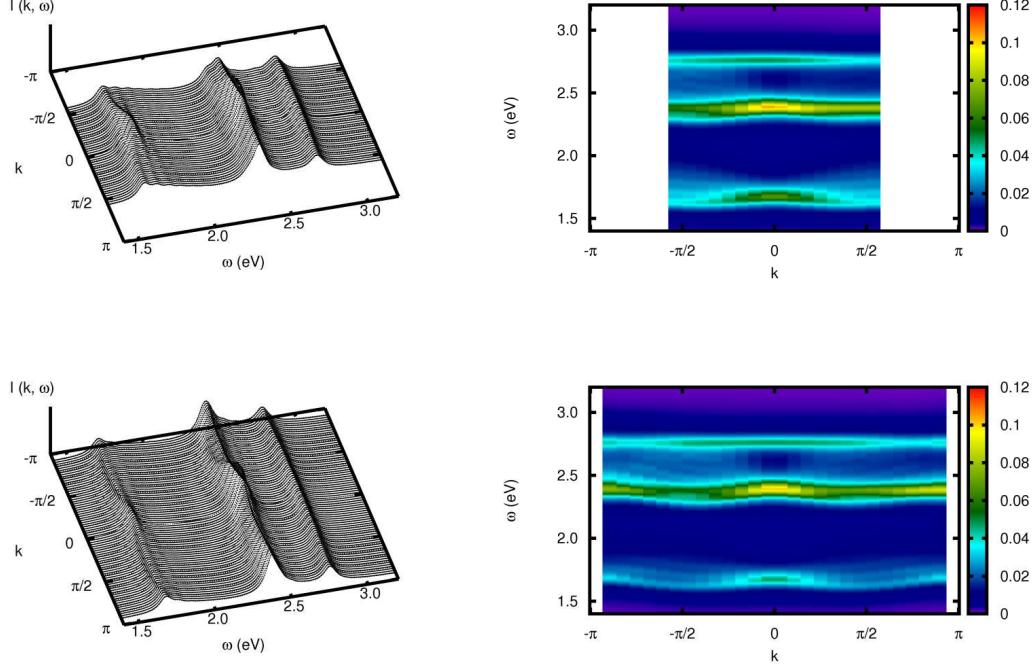


FIG. 8: (Color online) RIXS cross section for $\psi = 90^\circ$ ($\psi = 130^\circ$) scattering geometry as calculated in the spin-orbital separation scenario and convoluted with the results from the local model, Fig. 13, on the top (bottom) panel. Left (right) panels show line (color map) spectra. Results for broadening $\eta = 0.05$ eV (cf. caption of Fig. 6).

- The c orbiton spectrum: both the dispersion and the intensities agree qualitatively and quantitatively; in particular the theoretical spectrum has the largest intensity at $k = 0$ momentum which is solely a result of the dispersion originating in the spin-orbital separation scenario (the RIXS local matrix elements for the c orbiton are momentum-independent in the RIXS geometry of Fig. 7).
- The b orbiton dispersion: the dispersion has the same particular cosine-like shape with a period π and minima at $\pm\pi/2$; the spectral weights agree qualitatively and quantitatively.
- ‘Shadow’ (‘oval’-like) bands above the b orbiton: the width and shape of the shadow band is very similar both in the experiment and in theory; spectral weights agree relatively well (e.g. larger spectral weights for the negative than for the positive momentum transfer).

The characteristic spin-orbital separation spectrum is much better visible for the b orbiton than for the c orbiton. The reason for this is twofold. Firstly, the overall sensitivity of RIXS to the b orbiton excitations is much larger than to the c orbiton due to the chosen geometry of the RIXS experiment. Thus all features related to the b orbiton are better visible than those related to the c orbiton. Secondly, even despite this, the spin-orbital

separation can be better observed for the b orbiton case than for the c orbiton, cf. Fig. 6. This is because the effective hopping element t_b for the b orbiton is larger than the hopping t_c for the c orbiton, cf. Table I, which is due to: (i) the renormalization $\propto \lambda_c$ of the copper oxygen hopping t_π for the hopping from c orbiton due to the formation of the bonding and antibonding states with the neighboring oxygens (see App. A), and (ii) the larger effective charge transfer gap for the c orbital than for the b orbital (see Table I; note that this effective charge transfer gap is defined as the difference in energy between a particular $3d$ orbital and the *hybridizing* $2p$ orbital and thus is larger for lower lying $3d$ orbitals).

The main discrepancy between the experiment and theory is related to the somewhat smaller dispersion in the theoretical calculations than in the experiment. While there might be several reasons explaining this fact, let us point two plausible ones. Firstly, the neglected spin-orbit coupling in the $3d$ orbitals would mix the b and d (i.e. xz and yz) orbital excitations and would lead to a finite dispersion in the d orbital channel. This would mean that the present dispersionless d orbital excitation would no longer ‘cover’ parts of the dispersive b orbiton. Thus, effectively this would lead to large dispersive feature around the b and d excitation energy. Secondly, the relatively high covalency of the Sr_2CuO_3 compound, which is not taken into account in the present derivation,

might lead to the more itinerant character of the system and larger dispersion relation for the orbiton.

Comparison with other theoretical calculations.— There are actually two other simple approximations which might naively be employed to calculate the RIXS spectra and which could be compared against the experiment: (i) the ‘local model’ approximation which assumes that *all* orbital excitations are local, i.e. also both the *b* and the *c* orbiton spectral function do not have any momentum dependence (cf. Appendix C), and (ii) the one which assumes that the spectral functions of the *b* and *c* orbitons are calculated using the linear orbital wave approximation (cf. part 2 of Appendix B). However, as shown in detail in the above mentioned appendices, the RIXS spectra calculated using these approximations do not fit the experimental ones.

VI. DISCUSSION AND CONCLUSIONS

We first list a few alternative scenarios that might lead to the dispersive orbital excitations in Sr_2CuO_3 and argue why they do not lead to a plausible explanation of the experimental results reported in Ref. 22. At the end of the section we present our conclusions.

A. Alternative scenarios leading to dispersive features in the RIXS spectrum of Sr_2CuO_3

Spin-charge separation observed directly.— The spin-charge separation where a hole created in a 1D AF decays into a holon and a spinon can be observed with ARPES: e.g. in SrCuO_2 ⁶³ or in Sr_2CuO_3 ⁶⁷. However, not only that holon dispersion is much larger than the dispersion under consideration in this paper (it is of the order of 1.1 eV⁶⁷), but also – what is more important – one cannot directly probe the spin-charge separation in RIXS, since in RIXS the total charge is conserved⁶⁸.

Holon, antiholon and two spinons, i.e. spin-charge separation indirectly— Nevertheless, it occurs that there is a possibility to observe spin-charge separation with RIXS or EELS in an indirect way. If one transfers a hole from the copper site *i* either to the neighboring copper site *i* + 1 to form a doubly occupied site *or* to the neighboring oxygen plaquette surrounding the central copper site *i* + 1 to form a Zhang-Rice singlet, then one ends up with one hole in the spin background on site *i* and another hole in the spin background on site *i* + 1. Next, both of these objects can become mobile and experience the spin-charge separation: the first one can move by decaying to a holon and a spinon while the second one can move by decaying to an antiholon and a spinon. This rather complicated scenario was invoked to explain the *K* edge RIXS spectra in various quasi-1D cuprates (cf. Refs. 68,69) and the EELS spectrum in Sr_2CuO_3 ⁷⁰.

However, the common feature of all these experiments is that there is a large dispersion (of the order of 1 eV)

which has a periodicity of 2π and a minimum at $k = 0$. Thus, clearly it is not the spectrum that is observed in the *L* edge RIXS experiment in Ref. 22. The reason for this is that RIXS at *L* edge is much more sensitive to the on-site excitations on the copper site than to the intersite charge transfer excitations on the neighbouring oxygen or copper sites⁷¹.

Orbital excitations propagating via the $O(2p)$ orbitals.— In that case the propagation would entirely happen via the $O(2p)$ orbitals on a kind of a zigzag chain along the CuO_4 plaquettes. This, however, cannot lead to a momentum dependence in the observed spectrum.

Similar experiments.— One should also compare the here reported theoretical results to the experimental ones which were discussed in Ref. 72. There a somewhat similar dispersive feature, as the one discussed here, was discovered in the RIXS spectra at the $1s \rightarrow 3d$ edge. Although this dispersion was attributed to an orbital excitation, it remained unclear to the authors of that paper how to correctly interpret this phenomenon. An obvious suggestion is that the spectrum observed in Ref. 72 might be of similar origin as the one discussed here: the dispersion also has a π periodicity and is of the order of 0.2 eV. However, there are two problems with this scenario: (i) there is just one dispersive peak but no other dispersive modes and there is no shoulder peak, (ii) the dispersion is shifted by $\pi/2$ in the momentum space. This first problem can perhaps be ‘solved’: RIXS at the $1s \rightarrow 3d$ edge involves quadrupolar transitions, the RIXS signal is rather weak, and thus it is possible that one cannot observe all details of the spectra. However, the second one remains a challenge for theory. One suggestion might be that the effective ‘dispersion’ that one sees in the spectrum in Ref. 72 is the top part of the ‘shadow’ bands that we reported here for the *b* orbiton – this would require that the ‘true’ (lower) *b* orbiton band is covered by some other excitations in that experiment.

B. Conclusions

We have considered in detail the origin of the dispersive features observed in the RIXS spectra of the quasi-1D CuO_3 chain in Sr_2CuO_3 ²². We explained that these dispersive features can indeed be attributed to the dispersive orbital excitations (orbitons) – which actually were unambiguously observed for the first time. The unexpectedly strong dispersion of these excitations are not only a result of the relatively strong superexchange interactions in the system but also due to the fractionalization of the spin and orbital degrees of freedom which, as shown in this paper and in Refs. 22,49, is possible in this quasi-1D strongly correlated system.

Finally, one may wonder whether the spin-orbital separation phenomenon can also be observed in other transition metal oxides. While we suggest that this should be possible in most other quasi-1D system which are

again mostly cuprates, it is impossible to observe this phenomenon in 2D and 3D systems, such as La_2CuO_4 , LaMnO_3 or LaVO_3 , with long range magnetic order, cf. Ref. 73. However, many theoretical studies have discussed the nature of the orbital excitations in these systems which leaves large field to be still explored experimentally (cf. Refs. 11,13,17,35,37–42,45). Furthermore, the mapping of the spin-orbital model into the effective simpler t - J model presented here is actually valid also in higher dimensions⁴⁹. However, the lack of experimental results, which can verify various theories concerning these orbital excitations, means that it remains a challenge both for theory and for experiment to explore the nature of the orbital excitations in higher dimensions.

VII. ACKNOWLEDGMENTS

First and foremost we acknowledge very stimulating discussions and common work on this subject with

our theoretical collaborators Maria Daghofer, Liviu Hozoi, and Giniyat Khaliullin as well as with our experimental collaborators Justina Schlappa, Thorsten Schmit, and Henrik Ronnow. We also thank Stefan-Ludwig Drechsler, Andrzej M. Oleś, George A. Sawatzky, Michel van Veenendaal, and Victor Yushhankhai for very valuable comments. K.W. acknowledges support from the Alexander von Humboldt Foundation, the Polish National Science Center (NCN) under Project No. 2012/04/A/ST3/00331, and from the U.S. Department of Energy, Materials Sciences and Engineering Division, under Contract No. DE-AC02-76SF00515. This research benefited from the RIXS collaboration supported by the Computational Materials Science Network program of the Division of Materials Science and Engineering, US Department of Energy, grant no. DE-SC0007091.

-
- ¹ M. Imada, A. Fujimori, and Y. Tokura, *Rev. Mod. Phys.* **70**, 1039 (1998).
 - ² R. Coldea *et al.*, *Phys. Rev. Lett.* **86**, 5377 (2001).
 - ³ S. Notbohm *et al.*, *Phys. Rev. Lett.* **98**, 027403 (2007).
 - ⁴ I. A. Zaliznyak *et al.*, *Phys. Rev. Lett.* **93**, 087202 (2004).
 - ⁵ L. J. P. Ament *et al.*, *Phys. Rev. Lett.* **103**, 117003 (2009).
 - ⁶ M. W. Haverkort, *Phys. Rev. Lett.* **105**, 167404 (2010).
 - ⁷ L. Braicovich *et al.*, *Phys. Rev. Lett.* **102**, 167401 (2009).
 - ⁸ L. Braicovich *et al.*, *Phys. Rev. Lett.* **104**, 077002 (2010).
 - ⁹ A. Auerbach, *Interacting Electrons and Quantum Magnetism* (Springer, New York, 1994).
 - ¹⁰ T. Giamarchi, *Quantum Physics in One Dimension* (Oxford University Press, Oxford, 2004).
 - ¹¹ K. I. Kugel and D. I. Khomskii, *JETP* **37**, 725 (1973).
 - ¹² H. F. Pen, J. van den Brink, D. I. Khomskii, and G. A. Sawatzky, *Phys. Rev. Lett.* **78**, 1323 (1997).
 - ¹³ S. Ishihara and S. Maekawa, *Phys. Rev. B* **62**, 2338 (2000).
 - ¹⁴ F. Forte, L. J. P. Ament, and J. van den Brink, *Phys. Rev. Lett.* **101**, 106406 (2008).
 - ¹⁵ P. Marra, K. Wohlfeld, and J. van den Brink, *Phys. Rev. Lett.* **109**, 117401 (2012).
 - ¹⁶ Note that due to the typically quenched angular momentum of the orbital ordered ground state, neutrons cannot detect the orbital order, cf. Ref. 15.
 - ¹⁷ S. Ishihara, *Phys. Rev. B* **69**, 075118 (2004).
 - ¹⁸ S.-I. Shamoto *et al.*, *Journal of Neutron Research* **13**, 175 (2005).
 - ¹⁹ Y.-J. Kim *et al.*, *Phys. Rev. B* **84**, 085132 (2011).
 - ²⁰ E. Saitoh *et al.*, *Nature* **410**, 180 (2001).
 - ²¹ M. Grüninger *et al.*, *Nature* **418**, 39 (2002).
 - ²² J. Schlappa *et al.*, *Nature* **485**, 82 (2012).
 - ²³ R. M. Macfarlane and J. W. Allen, *Phys. Rev. B* **4**, 3054 (1971).
 - ²⁴ D. Polli *et al.*, *Nature Mater.* **6**, 643 (2007).
 - ²⁵ C. Ulrich *et al.*, *Phys. Rev. Lett.* **103**, 107205 (2009).
 - ²⁶ P. B. Allen and V. Perebeinos, *Phys. Rev. Lett.* **83**, 4828 (1999).
 - ²⁷ J. van den Brink, *Phys. Rev. Lett.* **87**, 217202 (2001).
 - ²⁸ K. P. Schmidt, M. Grüninger, and G. S. Uhrig, *Phys. Rev. B* **76**, 075108 (2007).
 - ²⁹ Note that this intersite spin-orbital interaction has nothing to do with the relativistic on-site spin-orbit interaction, which in the here discussed case of $3d$ transition metal oxides is vanishingly small with respect to the spin-orbital interaction^{55,57}.
 - ³⁰ A. M. Oleś, P. Horsch, L. F. Feiner, and G. Khaliullin, *Phys. Rev. Lett.* **96**, 147205 (2006).
 - ³¹ A. M. Oleś, *Journal of Physics: Condensed Matter* **24**, 313201 (2012).
 - ³² W. Brzezicki, J. Dziarmaga, and A. M. Oleś, *Phys. Rev. Lett.* **109**, 237201 (2012).
 - ³³ W. Brzezicki, J. Dziarmaga, and A. M. Oleś, *Phys. Rev. B* **87**, 064407 (2013).
 - ³⁴ K. I. Kugel and D. I. Khomskii, *Sov. Phys. Usp.* **25**, 231 (1982).
 - ³⁵ L. F. Feiner, A. M. Oleś, and J. Zaanen, *Phys. Rev. Lett.* **78**, 2799 (1997).
 - ³⁶ L. F. Feiner, A. M. Oleś, and J. Zaanen, *Journal of Physics: Condensed Matter* **10**, L555 (1998).
 - ³⁷ S. Ishihara, J. Inoue, and S. Maekawa, *Phys. Rev. B* **55**, 8280 (1997).
 - ³⁸ J. van den Brink *et al.*, *Phys. Rev. B* **58**, 10276 (1998).
 - ³⁹ A. M. Oleś, L. Felix Feiner, and J. Zaanen, *Phys. Rev. B* **61**, 6257 (2000).
 - ⁴⁰ G. Khaliullin and V. Oudovenko, *Phys. Rev. B* **56**, R14243 (1997).
 - ⁴¹ G. Khaliullin and S. Maekawa, *Phys. Rev. Lett.* **85**, 3950 (2000).
 - ⁴² K. Kikoin, O. Entin-Wohlman, V. Fleurov, and A. Aharony, *Phys. Rev. B* **67**, 214418 (2003).
 - ⁴³ K. Wohlfeld, A. M. Oleś, and P. Horsch, *Phys. Rev. B* **79**, 224433 (2009).
 - ⁴⁴ A. Herzog, P. Horsch, A. M. Oleś, and J. Sirker, *Phys. Rev. B* **83**, 245130 (2011).

- ⁴⁵ J. Kim *et al.*, Phys. Rev. Lett. **108**, 177003 (2012).
⁴⁶ W.-L. You, A. M. Oleś, and P. Horsch, Phys. Rev. B **86**, 094412 (2012).
⁴⁷ B. Kumar, Phys. Rev. B **87**, 195105 (2013).
⁴⁸ D. Vieira, Arxiv **1212.3241**, (2012).
⁴⁹ K. Wohlfeld *et al.*, Physical Review Letters **107**, 147201 (2011).
⁵⁰ T. Ami *et al.*, Phys. Rev. B **51**, 5994 (1995).
⁵¹ N. Motoyama, H. Eisaki, and S. Uchida, Phys. Rev. Lett. **76**, 3212 (1996).
⁵² K. M. Kojima *et al.*, Phys. Rev. Lett. **78**, 1787 (1997).
⁵³ R. Neudert *et al.*, Phys. Rev. B **62**, 10752 (2000).
⁵⁴ J. S. Griffith, *The Theory of Transition Metal Ions* (Cambridge University Press, Cambridge, 1964).
⁵⁵ A. M. Oleś, G. Khaliullin, P. Horsch, and L. F. Feiner, Phys. Rev. B **72**, 214431 (2005).
⁵⁶ J. B. Grant and A. K. McMahan, Phys. Rev. B **46**, 8440 (1992).
⁵⁷ M. W. Haverkort, *Spin and Orbital Degrees of Freedom in Transition Metal Oxides and Oxide Thin Films Studied by Soft X-ray Absorption Spectroscopy* (University of Cologne PhD Thesis, Cologne, 2005).
⁵⁸ J. Zaanen and A. M. Oleś, Phys. Rev. B **37**, 9423 (1988).
⁵⁹ M. W. Haverkort, M. Zwierzycki, and O. K. Andersen, Phys. Rev. B **85**, 165113 (2012).
⁶⁰ Let us note that these two different formulae for the orbital spectral functions are not fully equivalent: Eqs. (24)-(25) do not contain the orbital excitations which are above the Hubbard gap. However, we can safely neglect the coherent propagation of the orbital excitations in the Hilbert space *with* double occupancies, since: (i) for the coherent propagation of the orbital excitations the relevant gap is of the order of the Hubbard U and not of the order of the charge transfer gap Δ , and (ii) $\bar{\epsilon}_b$ and $\bar{\epsilon}_c$ are much small than the Hubbard U .
⁶¹ G. Martinez and P. Horsch, Phys. Rev. B **44**, 317 (1991).
⁶² P. Bouillot *et al.*, Phys. Rev. B **83**, 054407 (2011).
⁶³ C. Kim *et al.*, Phys. Rev. Lett. **77**, 4054 (1996).
⁶⁴ J. Luo, G. T. Trammell, and J. P. Hannon, Phys. Rev. Lett. **71**, 287 (1993).
⁶⁵ F. M. F. De Groot, P. Kuiper, and G. A. Sawatzky, Phys. Rev. B **57**, 14584 (1998).
⁶⁶ J. Schlappa and T. Schmitt (private communication).
⁶⁷ H. Fujisawa *et al.*, Phys. Rev. B **59**, 7358 (1999).
⁶⁸ Y.-J. Kim *et al.*, Phys. Rev. Lett. **92**, 137402 (2004).
⁶⁹ M. Z. Hasan *et al.*, Phys. Rev. Lett. **88**, 177403 (2002).
⁷⁰ R. Neudert *et al.*, Phys. Rev. Lett. **81**, 657 (1998).
⁷¹ J. Geck and V. Bisogni (private communication).
⁷² J. W. Seo *et al.*, Phys. Rev. B **73**, 161104 (2006).
⁷³ K. Wohlfeld, M. Daghofer, G. Khaliullin, and J. van den Brink, J. Phys.: Conf. Ser. **391**, 012168 (2012).
⁷⁴ J. H. Jefferson, H. Eskes, and L. F. Feiner, Phys. Rev. B **45**, 7959 (1992).
⁷⁵ F. Moussa *et al.*, Phys. Rev. B **54**, 15149 (1996).
⁷⁶ K. Wohlfeld, M. Daghofer, A. M. Oleś, and P. Horsch, Phys. Rev. B **78**, 214423 (2008).
⁷⁷ If we were to make a similar analysis as above but for the spin sector of the ground state $|\Phi\rangle$ being a Neel AF instead of the quantum AF, we would notice that A and B2 processes are not present in that case and it is only the B1 process which contributes. Thus, we see that in that case the LOW approach works fine.

Appendix A: Reduction of the effective hopping in the linear chain due to $\propto t_n^2$ perturbative processes

Let us firstly state that, due to the t_n^2 processes, the number of holes residing in the orbitals *within* the Cu-O-Cu-O-... chain for a particular CuO₄ cluster depends on the particular α orbital forming the bonding state, cf. Fig. 1. More precisely, for the bonding states formed around the b orbital and occupied by one hole the whole charge is concentrated in the orbitals within the Cu-O-Cu-O-... chain, while for the bonding states formed by the a or c orbitals it is not the case. This is because, in the latter case the bonding state is formed by orbitals situated above and below the Cu-O-Cu-O-... chain.

Looking in detail at this problem we concentrate first at the case with the hole being initially doped into the a orbital. The part of the charge transfer Hamiltonian (1) which is responsible for the effect mentioned above is:

$$-t_{\sigma o} \sum_{i,\sigma} \left(f_{ia\sigma}^\dagger f_{iy o+\sigma} - f_{ia\sigma}^\dagger f_{iy o-\sigma} + \text{H.c.} \right) + \Delta_{yo} \sum_i (n_{iy o+} + n_{iy o-}), \quad (\text{A1})$$

with $t_{\sigma o}$ being the main ‘actor’ here, i.e. it is this hopping element which makes the hole escape from the Cu-O-Cu-O-... chain (see Fig. 1). We can now easily diagonalize this three-level problem and calculate the number of holes left in the a orbital by evaluating the following quantum mechanical amplitude

$$\lambda_a \equiv \langle a | \psi_a \rangle = \frac{\Delta_{yo} - e_a}{\sqrt{2t_{\sigma o}^2 + (\Delta_{yo} - e_a)^2}}, \quad (\text{A2})$$

where $e_a = (\Delta_{yo} - \sqrt{\Delta_{yo}^2 + 8t_{\sigma o}^2})/2$, while $|\psi_a\rangle$ is the bonding state coming from the above diagonalization procedure and which is well separated from the antibonding and nonbonding states (so that we can skip the latter two when studying the low energy regime).

A similar analysis as above but for the c orbital leads to

$$\lambda_c \equiv \langle c | \psi_c \rangle = \frac{\Delta_{xo} - e_c}{\sqrt{2t_{\pi o}^2 + (\Delta_{xo} - e_c)^2}}, \quad (\text{A3})$$

where $e_c = (\Delta_{xo} - \sqrt{\Delta_{xo}^2 + 8t_{\pi o}^2})/2$. Here again $|\psi_c\rangle$ is the bonding state but this time centered around the c orbital.

Finally, since the b orbital does not hybridize with the oxygens lying above or below the Cu-O-Cu-O-... chain, the corresponding λ_b would be equal to unity and could be skipped in what follows.

These renormalized values of the number of holes within the chain directly lead to renormalized values of the hopping elements from the ψ_a and ψ_c orbitals with respect to the hopping elements from the pure a and c orbitals. A rigorous calculation would now require that together with using the parameters λ_a and λ_c as renormalizing the hopping, we should also use the basis spanned

by the ψ_a and ψ_c orbitals. However, we avoid this in our calculations. We justify this ‘approximation’ as follows:

In general, to properly account for *all* the effects arising from the $\propto t_n^2$ perturbative processes, the rigorous treatment would require using the so-called cell perturbation theory⁷⁴: that is to rewrite the full charge transfer Hamiltonian using the bonding / antibonding states and then to calculate the superexchange interactions in this basis. This, however, requires very tedious calculations as even for the much simpler case of Ref. 74 the problem is nontrivial and complex.

Therefore, we follow the more standard route, i.e. we calculate the superexchange interactions in Secs. III B–III E using the orbital basis that was already used to write down the charge transfer model Eq. (1). The only two remnants of the cell perturbation theory, or in other words of the fact that the superexchange should be modified due to the formation of bonding and antibonding states, are: (i) the use of the renormalized parameters $\bar{\varepsilon}_\alpha$ instead of ε_α as discussed in Sec. III A, and (ii) the use of the factors λ_a and λ_c which renormalize the number of holes present within the chain when a hole is doped into a or c orbital, respectively (see above). We have verified that the renormalization of other parameters has a much smaller effect. In particular: (i) the charge transfer energies in the bonding states should change similarly for all orbitals with respect to their values in the charge transfer model defined in the $2p$ and $3d$ orbital basis, (ii) the matrix elements of the Coulomb interaction in the bonding / antibonding basis are similar to the ones calculated in the $2p$ and $3d$ orbital basis.

Appendix B: Linear orbital wave approximation

The ‘standard’ way to obtain the orbiton dispersion, in the spin-orbital model is to use the linear orbital wave (LOW) approximation (cf. Ref. 43) for the orbital pseudospin degrees of freedom and to integrate out the spin degrees of freedom in a mean-field way⁴⁹. This in general *may* be justified here due to the presence of the long range orbital order. In order to test this scenario, in this section of the appendix, we perform the LOW approximation and calculate the orbiton spectral function (see part 1 below) together with the RIXS cross section (see part 2 below). We also discuss why the LOW approximation fails in properly describing the experimental results reported in Ref. 22, cf. part 3 below.

1. Spectral function in linear orbital wave approximation

LOW for b orbiton.— Following e.g. Ref. 43 and Ref. 49 we first introduce the following bosonic creation (annihilation) operators β_j^\dagger (β_j) for the orbital pseu-

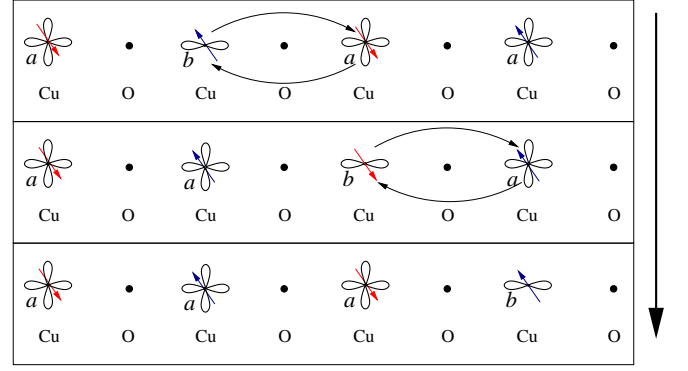


FIG. 9: (Color online) Schematic view of the propagation of the orbiton in the LOW approximation: note that the orbiton moves in such a way that it does not disturb the AF correlations which is due to the mean-field decoupling of spin and orbital degrees of freedom.

dospin operator:

$$\begin{aligned}\sigma_j^z &= \beta_j^\dagger \beta_j - \frac{1}{2}, \\ \sigma_j^+ &= \beta_j^\dagger, \\ \sigma_j^- &= \beta_j,\end{aligned}\tag{B1}$$

where we already skipped the three-orbiton terms in the above expressions, since we will keep only quadratic terms in the bosonic degrees of freedom in the effective Hamiltonian below. Besides, we decouple the orbital operators from the spins and assume for the spins their appropriate mean field values. The latter is a standard procedure when calculating the spin wave dispersion in the spin and orbitally ordered systems^{55,75}. Applying these transformations to the Hamiltonian $\bar{\mathcal{H}}$ we obtain the following LOW Hamiltonian:

$$\begin{aligned}H_{\text{LOW}}^{ab} &\equiv H_{\text{LOW}}^0 + H_{\text{LOW}}^a + H_{\text{LOW}}^b = \sum_k (B + 2J_b \cos k) \\ &\times \beta_k^\dagger \beta_k + J_1(1+R) \sum_i \left(\mathbf{S}_i \cdot \mathbf{S}_{i+1} - \frac{1}{4} \right),\end{aligned}\tag{B2}$$

with the constants B and J_b defined as

$$\begin{aligned}B &\equiv \bar{\varepsilon}_b - \mathcal{A}(R_1^b J_{12}^b + r_1^b \frac{J_1 + J_2}{2}) - \mathcal{B}(R_2^b J_{12}^b + r_2^b \frac{J_1 + J_2}{2}) \\ &+ 2J_1(1+R)\mathcal{B}\end{aligned}\tag{B3}$$

and

$$J_b \equiv \frac{1}{2} J_{12}^c [\mathcal{A}(R_1^b + r_1^b) - \mathcal{B}(R_2^b + r_2^b)],\tag{B4}$$

with

$$\mathcal{A} \equiv \langle \Phi | \mathbf{S}_i \cdot \mathbf{S}_{i+1} + \frac{3}{4} | \Phi \rangle,\tag{B5}$$

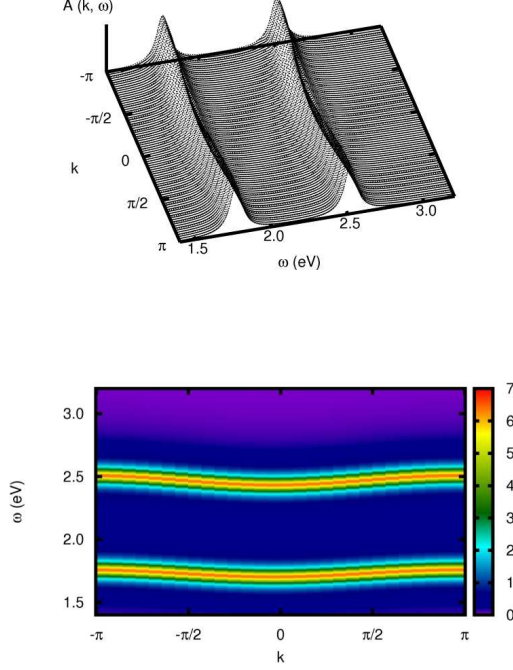


FIG. 10: (Color online) Spectral function $A_b(k, \omega) + A_c(k, \omega)$ as a function of momentum k and energy transfer ω in the LOW approximation and quantum AF case. Results for broadening $\eta = 0.05$ eV (cf. caption of Fig. 6).

and

$$\mathcal{B} \equiv \left\langle \Phi \left| \frac{1}{4} - \mathbf{S}_i \cdot \mathbf{S}_{i+1} \right| \Phi \right\rangle. \quad (\text{B6})$$

Here $|\Phi\rangle$ is the AF and FO ground state (cf. Sec. IV) of H_{LOW}^b with energy E_Φ . The values of the spin-spin correlations have to be calculated for the spin ground state of the Hamiltonian H_{LOW}^b which is a quantum AF, see Sec. IV. This can easily be obtained from the well-known exact Bethe-Ansatz-based solution for a 1D quantum AF: $\mathcal{A} = 0.31$ and $\mathcal{B} = 0.69$. (Let us note that these numbers are significantly different from the ones that are known for the not-realized-here ‘classical’ case, i.e. for the ordered Neel AF – in that case: $\mathcal{A} = 0.5$, $\mathcal{B} = 0.5$, and $J_b \simeq 0.011$ eV.) Using the spin-orbital model parameters from Table I, we finally obtain $J_b \simeq -0.019$ eV as also reported in Table I.

Although one could directly use Eq. (B3) to calculate the on-site cost of an orbital excitation B , this value can also be calculated by using the *ab-initio* quantum chemistry calculation for a *ferromagnetic* chain with four CuO_3 plaquettes. The latter gives the value of a single orbital excitation in the ferromagnetic chain $E_b = 2.15$ eV (cf. discussion in Sec. IV and Table I) and leads to

$$B \simeq E_b + E_{\text{AF}} \quad (\text{B7})$$

and, since $E_{\text{AF}} = 0.33$ eV, $B \simeq 2.48$ eV, cf. Table I. To be in line with Ref. 22, we use the latter value as the cost of the local b orbital excitations in the AF chain.

Having defined the Hamiltonian and its parameters, we are now ready to compute the orbiton spectral function $A_b(k, \omega)$ [Eq. (24)], which, when expressed in the new bosonic operators [Eq. (B1)], reads

$$A_b(k, \omega) = \frac{1}{\pi} \lim_{\eta \rightarrow 0} \Im \langle \Phi | \beta_k \frac{1}{\omega + E_\Phi - H_{\text{LOW}}^{ab} - i\eta} \beta_k^\dagger | \Phi \rangle. \quad (\text{B8})$$

Since $|\Phi\rangle$ is a vacuum for boson operators $\beta|\Phi\rangle = 0$, we easily obtain

$$A_b(k, \omega) = \frac{1}{\pi} \lim_{\eta \rightarrow 0} \Im \frac{1}{\omega - B - 2J_b \cos k - i\eta}. \quad (\text{B9})$$

The orbiton spectral function consists of a single quasi-particle peak with a sine-like dispersion, with period 2π and bandwidth $4|J_b| \simeq 0.08$ eV, cf. Fig. 10. This result can be intuitively understood by looking at the cartoon picture of the orbiton propagation in the LOW approximation, cf. Fig. 9.

LOW for c orbiton.— Following the same steps as above we obtain:

$$\begin{aligned} H_{\text{LOW}}^{ac} \equiv & H_{\text{LOW}}^0 + H_{\text{LOW}}^a + H_{\text{LOW}}^c = \sum_k (C + 2J_c \cos k) \\ & \times \beta_k^\dagger \beta_k + J_1(1 + R) \sum_i \left(\mathbf{S}_i \cdot \mathbf{S}_{i+1} - \frac{1}{4} \right) \end{aligned} \quad (\text{B10})$$

with the constants C and J_c defined as

$$\begin{aligned} C \equiv & \bar{\epsilon}_c - \mathcal{A}(R_1^c J_{12}^c + r_1^c \frac{J_1 + J_2^c}{2}) - \mathcal{B}(R_2^c J_{12}^c + r_2^c \frac{J_1 + J_2^c}{2}) \\ & + 2J_1(1 + R)\mathcal{B} \end{aligned} \quad (\text{B11})$$

and

$$J_c \equiv \frac{1}{2} J_{12}^c [\mathcal{A}(R_1^c + r_1^c) - \mathcal{B}(R_2^c + r_2^c)]. \quad (\text{B12})$$

which gives $J_c \simeq -0.014$ eV, cf. Table I. Again $C \simeq 1.74$ eV can be estimated using the *ab-initio* calculated value (cf. discussion above for the b orbiton) of $E_c \simeq 1.41$ eV for a local c orbital excitation in the ferromagnetic chain and the relation (see above)

$$C \simeq E_c + E_{\text{AF}}. \quad (\text{B13})$$

Finally, we obtain the following spectral function $A_c(k, \omega)$

$$A_c(k, \omega) = \frac{1}{\pi} \lim_{\eta \rightarrow 0} \Im \frac{1}{\omega - C - 2J_c \cos k - i\eta}, \quad (\text{B14})$$

which is also shown in Fig. 10 and which qualitatively resembles the above calculated b orbiton dispersion.

Spin-orbital waves.— As a side remark, let us note that the joint spin-orbital wave defined as in Ref. 39 cannot be present in the considered spin-orbital model. The reason is that this would require such terms as e.g. $(S_i^+ S_j^- + S_i^- S_j^+)(\tau_i^+ \tau_j^+ + \tau_i^- \tau_j^-)$ to be present in the spin-orbital Hamiltonian (6) – which is not the case here.

2. RIXS in linear orbital wave scenario

In order to calculate RIXS cross section in the LOW approximation we first express the RIXS operator Eq. (47) in terms of the orbital pseudospins. For the b orbiton case (i.e. T_b operator), following Eq. (8) and Eq. (13), we obtain

$$T_b = \frac{1}{\sqrt{N}} \sum_j e^{ikj} [(B_{\uparrow,\uparrow} + B_{\downarrow,\downarrow}) \frac{1}{2} \sigma_j^+ + (B_{\uparrow,\uparrow} - B_{\downarrow,\downarrow}) S_j^z \sigma_j^+ + B_{\uparrow,\downarrow} S_j^+ \sigma_j^+ + B_{\downarrow,\uparrow} S_j^- \sigma_j^+] \quad (\text{B15})$$

Next, following Eq. (B1), we express the *first term* of the above written RIXS operator in terms of the Holstein-Primakoff bosons β_k^+

$$T_b^{(1)} = \frac{1}{2} (B_{\uparrow,\uparrow} + B_{\downarrow,\downarrow}) \beta_k^+. \quad (\text{B16})$$

Note that in the above expression the spin-dependent part [the three last terms of the right hand side of Eq. (B15)] in Eq. (B16) is skipped. This is because it does not lead to any dispersive excitations since there are no terms in the LOW Hamiltonian which could move a spin excitation together with an orbital excitation (in the LOW approximation). (This is somewhat similar to the problem of a hole doped into the orbitally ordered state in a 1D chain which can ‘visit’ the neighbouring sites but which spectrum is k -independent⁷⁶.) However, these three neglected terms will contribute to the total RIXS cross section as dispersionless excitations.

When, apart from the above discussed b orbiton case, we also include the contribution from the c orbiton (which is analogous to the b orbiton case) and from the dispersionless d and e orbitons, we obtain

$$\begin{aligned} I(k, \omega) = & \frac{1}{4} |B_{\uparrow,\uparrow} + B_{\downarrow,\downarrow}|^2 A_b(k, \omega) \\ & + \left(\frac{1}{4} |B_{\uparrow,\uparrow} - B_{\downarrow,\downarrow}|^2 + |B_{\downarrow,\uparrow}|^2 \right) \delta(\omega - E_b - E_{AF}) \\ & + \frac{1}{4} |C_{\uparrow,\uparrow} + C_{\downarrow,\downarrow}|^2 A_c(k, \omega) \\ & + \left(\frac{1}{4} |C_{\uparrow,\uparrow} - C_{\downarrow,\downarrow}|^2 + |C_{\downarrow,\uparrow}|^2 \right) \delta(\omega - E_c - E_{AF}) \\ & + (|D_{\uparrow,\uparrow}(k)|^2 + |D_{\downarrow,\downarrow}(k)|^2) \delta(\omega - E_d - E_{AF}) \\ & + (|E_{\uparrow,\uparrow}(k)|^2 + |E_{\downarrow,\downarrow}(k)|^2) \delta(\omega - E_e - E_{AF}). \end{aligned} \quad (\text{B17})$$

Here the spectral functions $A_b(k, \omega)$ and $A_c(k, \omega)$ are calculated in part 1 of Appendix B and the RIXS matrix elements follow from Sec. V A.

Comparison with the experiment.— The RIXS cross section calculated using Eq. (B17) is shown in Fig. 11. A small dispersion of the orbiton excitations, known already from the spectral functions in part 1 of Appendix B, is relatively well visible in the RIXS cross section. However, there is a *qualitative* disagreement between these theoretical calculations and the experimental results, cf. Fig. 4(a) in Ref. 22 for the case of the

RIXS with scattering angle $\Psi = 130^\circ$; a similar disagreement is obtained for the unpublished RIXS experimental results⁶⁶ for the scattering angle $\Psi = 90^\circ$. The main differences are as follows: (i) the theoretical dispersion has its minimum at $k = 0$ according to the calculations while this is not the case in the experiment, (ii) the theoretical results do not predict the onset of a continuum above the b excitation, (iii) the obtained dispersion of the quasiparticle peaks is much smaller than in the experiment, and (iv) there is a disagreement between the calculated and measured RIXS intensities.

3. Why linear orbital wave approximation fails

General considerations.— Let us show why the LOW theory, employed above in calculating the orbiton spectral function, cannot correctly reproduce the orbiton propagation in the here discussed spin-orbital model.

In order to do that, we take a closer look at all possible channels of the orbiton propagation, see Fig. 12, and calculate their relative contribution to the orbiton propagation in the LOW approximation. (In what follows we concentrate on the b orbiton case but similar arguments apply to the c orbiton case.) Thus, we split the effective orbiton superexchange process $\propto J_b$, as calculated in the previous section Eq. (B12), into three different contributions:

$$J_b = t_A + t_{B1} + t_{B2}, \quad (\text{B18})$$

where

$$t_A = \frac{1}{2} J_{12}^b (R_1^b + r_1^b + R_2^b + r_2^b) \left\langle \Phi \left| \frac{1}{2} (S_i^+ S_{i+1}^- + h.c.) \right| \Phi \right\rangle, \quad (\text{B19})$$

and

$$\begin{aligned} t_B = t_{B1} + t_{B2} = & \frac{1}{2} J_{12}^c [(R_1^b + r_1^b) \left\langle \Phi \left| S_i^z S_{i+1}^z + \frac{3}{4} \right| \Phi \right\rangle \\ & - (R_2^b + r_2^b) \left\langle \Phi \left| \frac{1}{4} - S_i^z S_{i+1}^z \right| \Phi \right\rangle], \end{aligned} \quad (\text{B20})$$

with

$$\begin{aligned} t_{B1} = & \frac{1}{2} J_{12}^b \mu [(R_1^b + r_1^b) \left\langle \uparrow\downarrow \left| S_i^z S_{i+1}^z + \frac{3}{4} \right| \uparrow\downarrow \right\rangle \\ & - (R_2^b + r_2^b) \left\langle \uparrow\downarrow \left| \frac{1}{4} - S_i^z S_{i+1}^z \right| \uparrow\downarrow \right\rangle], \end{aligned} \quad (\text{B21})$$

and

$$t_{B2} = \frac{1}{2} J_{12}^b (R_1^b + r_1^b) \nu \left\langle \downarrow\downarrow \left| S_i^z S_{i+1}^z + \frac{3}{4} \right| \downarrow\downarrow \right\rangle, \quad (\text{B22})$$

where $|\downarrow\downarrow\rangle$ denotes a ferromagnetic state, $|\uparrow\downarrow\rangle$ denotes a Neel AF state, and $\mu = |\langle \Phi | \uparrow\downarrow \rangle|^2 \sim 0.8$ and $\nu = |\langle \Phi | \downarrow\downarrow \rangle|^2 \sim 0.2$. Substituting parameters from Table I and spin correlations for the quantum AF, Neel AF, and ferromagnetic state we obtain that $t_A \sim -0.046$ eV, $t_{B1} \sim 0.009$ eV, and $t_{B2} \sim 0.018$ eV (one can check that

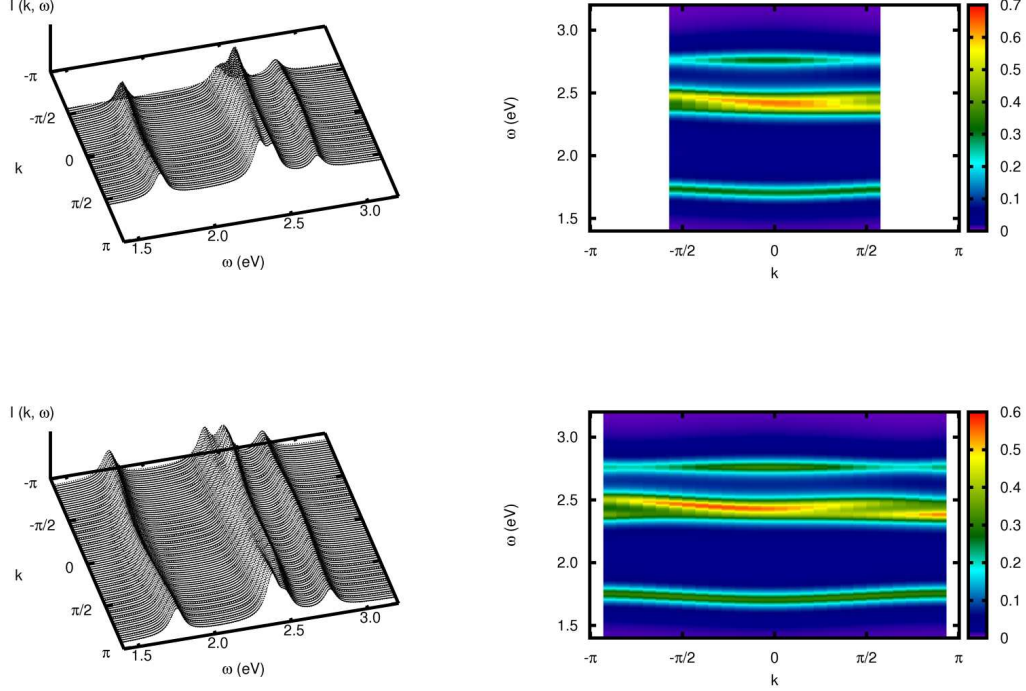


FIG. 11: (Color online) RIXS cross section for 90° (130°) scattering geometry as calculated in the LOW approximation and convoluted with the results from the local model, Fig. 13, on the top (bottom) panel. Left (right) panels show line (color map) spectra. Results for broadening $\eta = 0.05$ eV (cf. caption of Fig. 6).

altogether they indeed give $J_b \sim -0.019$ eV as calculated in the previous section, cf. Table I). Thus, we see that: (i) the A process has a surprisingly large contribution and an opposite sign to the other processes – so, unlike in the LOW result presented above, we should treat it separately as we make a huge error when we add all of these processes together, (ii) the B1 process is not only much smaller than the A process but also it is twice smaller than the B2 process⁷⁷.

This means that it is reasonable to try to define such an approximation, when calculating the orbiton propagation in the spin-orbital model (6), that, unlike the LOW approximation, will not average over these three processes. At the same time, such approximation could neglect the B1 process due to its relatively small amplitude. In order to verify what kind of approximation can be used, let us try to intuitively understand the difference between these three processes, cf. Fig. 12. While process A denotes an orbiton hopping accompanied by a spin flip, the B processes describe orbiton hoppings without any change in the spin background: the B1 for the case when the spins on the bond are antiparallel, while the B2 when the spins are parallel. However, one can also look at this problem in a different way: for the A and B2 process the spin of the hole in orbital b is conserved during the spin-orbital exchange. Hence, when process B1 is neglected, one can safely assume that the spin of the hole in the excited or-

biton does not change during orbiton propagation – and this is the essence of the mapping to the t - J model discussed in the main text of the paper.

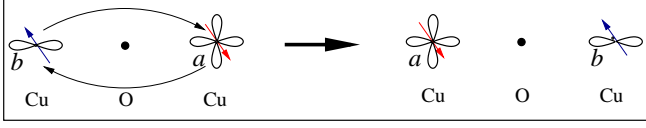
Appendix C: RIXS for dispersionless orbital excitations

In order to verify that the RIXS cross section in the so-called ‘local model’, i.e. with *all* orbital excitations dispersionless, indeed does not follow the experimental RIXS cross section²², we study the RIXS response for the following ‘local’ Hamiltonian

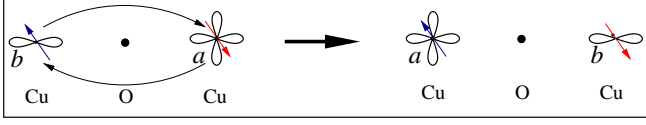
$$\begin{aligned} \mathcal{H} = & (E_b + E_{AF}) \sum_i (n_{ib} - n_{ia}) \\ & + (E_c + E_{AF}) \sum_i (n_{ic} - n_{ia}) \\ & + (E_d + E_{AF}) \sum_i (n_{id} - n_{ia}) \\ & + (E_e + E_{AF}) \sum_i (n_{ie} - n_{ia}). \end{aligned} \quad (C1)$$

Here E_b , E_c , E_d , and E_e are the costs of the local orbital excitations as calculated using the *ab-initio* quantum chemistry cluster calculations for the *ferromagnetic*

A PROCESS



B1 PROCESS



B2 PROCESS

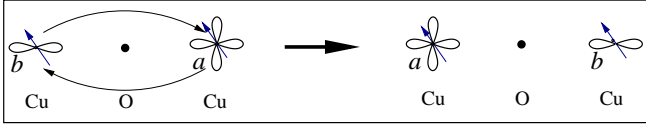


FIG. 12: (Color online) Schematic view of the three possible superexchange processes which lead to the orbiton propagation (here shown for the b orbiton but the c orbiton case is analogous). In the LOW approximation all of these processes, which amplitudes have different signs, are summed up. When treated separately, as in the spin-orbital separation approach, it occurs that for the orbiton propagation in a quantum AF only processes A and B2 matter.

CuO_3 chain in Sr_2CuO_3 (see Table I), while $E_{AF} = 0.24$ eV is the estimated correction to these values due to the quantum AF ground state (see Table I). Substituting Eq. (C1) into Eq. (46) and using Eq. (47) we easily obtain

$$\begin{aligned}
 I(k, \omega) = & (|B_{\uparrow, \uparrow}(k)|^2 + |B_{\uparrow, \downarrow}(k)|^2) \delta(\omega - E_b - E_{AF}) \\
 & + (|C_{\uparrow, \uparrow}(k)|^2 + |C_{\uparrow, \downarrow}(k)|^2) \delta(\omega - E_c - E_{AF}) \\
 & + (|D_{\uparrow, \uparrow}(k)|^2 + |D_{\uparrow, \downarrow}(k)|^2) \delta(\omega - E_d - E_{AF}) \\
 & + (|E_{\uparrow, \uparrow}(k)|^2 + |E_{\uparrow, \downarrow}(k)|^2) \delta(\omega - E_e - E_{AF}), \tag{C2}
 \end{aligned}$$

which is shown in Fig. 13 for the two discussed scattering geometries. It can be easily verified that the cross section calculated in this way does not agree with the RIXS experimental cross section, as shown in Fig. 4(a) in Ref. 22 (for the case of the scattering angle $\Psi = 130^\circ$; a similar disagreement is obtained for the unpublished RIXS experimental results⁶⁶ for the scattering angle $\Psi = 90^\circ$).

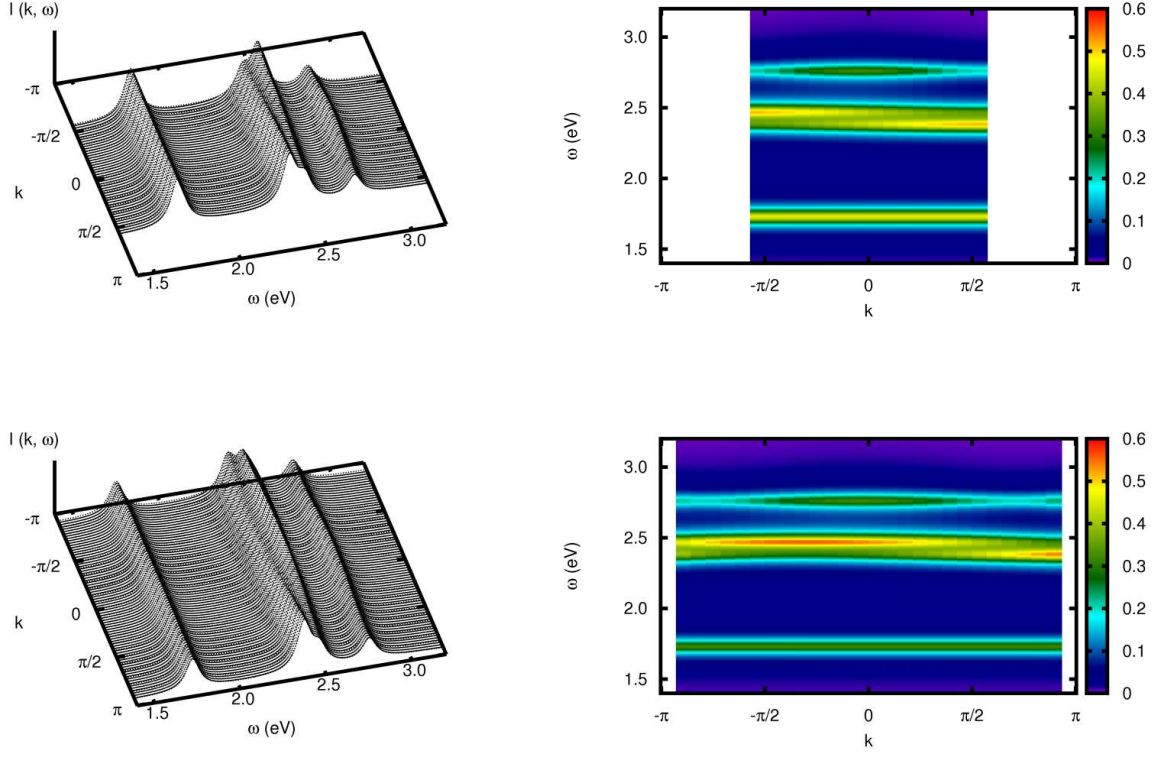


FIG. 13: (Color online) RIXS cross section for 90° (130°) scattering geometry as calculated in the local model on the top (bottom) panel. Left (right) panels show line (colour map) spectra. Results for broadening $\eta = 0.05$ eV (cf. caption of Fig. 6).